Stem Cell Reports
Article

OPEN ACCESS

Distinct Requirements for Extracellular and Intracellular MMP12 in the Development of the Adult V-SVZ Neural Stem Cell Niche

Xiwei Shan,[1] Lyl Tomlinson,[1] Qian Yang,[1] and Holly Colognato[1,*]
[1]Department of Pharmacological Sciences, Stony Brook University, Stony Brook, NY 11794, USA
*Correspondence: holly.colognato@stonybrook.edu
https://doi.org/10.1016/j.stemcr.2018.01.038

SUMMARY

The regulatory mechanisms that control neural stem cell (NSC) activation in the adult ventricular-subventricular zone (V-SVZ) stem cell niche have been the focus of intense investigation, yet how the niche first develops and organizes is poorly understood. Here, we examined matrix metalloproteinases (MMPs) for potential roles in V-SVZ stem cell niche development. MMP12 was found to promote appropriate niche cellular arrangements, the formation of specialized niche extracellular matrix, and the translational planar cell polarity of ependymal cells that surround and support niche NSCs. Surprisingly, ependymal cells were found to have an intracellular pool of MMP12 that promoted ependymal cell ciliogenesis by upregulating FOXJ1. In addition, both extracellular and intracellular MMP12 were found to regulate V-SVZ niche output by promoting NSC quiescence. These findings reveal that extracellular and intracellular MMP12 have both unique and overlapping roles that help orchestrate the development of the adult V-SVZ stem cell niche.

INTRODUCTION

Stem cells often reside in specialized microenvironments, or niches, where resident support cells, growth factors, and extracellular matrix (ECM) proteins regulate stem cell behaviors, including quiescence, proliferation, and differentiation (Brizzi et al., 2012). One such niche resides in the adult ventricular zone (VZ) of the mammalian brain, consisting of adult neural stem cells (NSCs) whose apical processes are surrounded by a "pinwheel" of multiciliated ependymal cells (ECs) (Mirzadeh et al., 2008), whose specialized cell-cell contacts help to regulate NSC functions (Lehtinen and Walsh, 2011; McClenahan et al., 2016; Paez-Gonzalez et al., 2011). In addition, ECM aggregates, or hubs, are localized by the ECM receptor dystroglycan at the junctions between ECs and NSCs in the apical VZ (McClenahan et al., 2016; Shen et al., 2008). Beneath the EC pinwheels, in the subventricular zone (SVZ), NSC basal processes contact vascular basal lamina via α6-containing integrins (Shen et al., 2008). Together, these and other cell-cell and cell-ECM arrangements in the ventricular-subventricular zone (V-SVZ) are thought to be critical for postnatal stem cell activation and regulated postnatal neurogenesis and gliogenesis (McClenahan et al., 2016; Mercier et al., 2002; Relucio et al., 2012; Shen et al., 2008).

The adult V-SVZ niche emerges postnatally in rodents. Shortly after birth, radial glial cells, which serve as embryonic NSCs, begin to transition into both adult NSCs and ECs. ECs achieve a planar cell polarity whereby the basal bodies of their motile cilia polarize on their apical surfaces, which is essential for the coordinated ciliary movements that direct cerebrospinal fluid (CSF) circulation and regulate neuroblast migration (Mirzadeh et al., 2010b; Sawamoto et al., 2006). During this time, ECs and NSCs arrange into cellular pinwheels, and diffusely distributed ECM on ECs transitions into aggregated ECM hubs at the interface of ECs and NSCs (McClenahan et al., 2016).

Given the dramatic reorganization of cellular and extracellular structures that take place in the postnatal V-SVZ, we hypothesized that matrix metalloproteinases (MMPs), a family of extracellular endopeptidases, may be important in this process. The 24 mammalian MMPs are mostly secreted or membrane-tethered proteins that cleave ECM proteins, cell adhesion molecules, and growth factors (Nagase et al., 2006). Due to the wide range of substrate selectivity, their expression, secretion, and activation are tightly controlled in a cellular and developmental fashion (Page-McCaw et al., 2007). MMPs have been shown to regulate the development and function of other stem cell niches, e.g., the hematopoietic stem cell niche and the mammary gland epithelial stem cell niche (Heissig et al., 2002; Kessenbrock et al., 2013; Nishida et al., 2012). In the adult V-SVZ, MMP24 (MT5-MMP) has been found to co-localize with NSCs and control their quiescence, in both physiological and pathological states, by cleaving N-cadherin (Porlan et al., 2014). However, whether MMPs regulate the postnatal development of the V-SVZ NSC niche itself remains largely unknown.

In this study, we sought to understand how MMPs contribute to the development and function of the postnatal V-SVZ stem cell niche. We characterized MMP family expression during the NSC-to-EC transition and found MMP12 to be highly upregulated during this process, and that ECs can express an intracellular MMP12. Using an *Mmp12* mutant mouse with a selective loss of the secreted, extracellular MMP12, we explored the functions

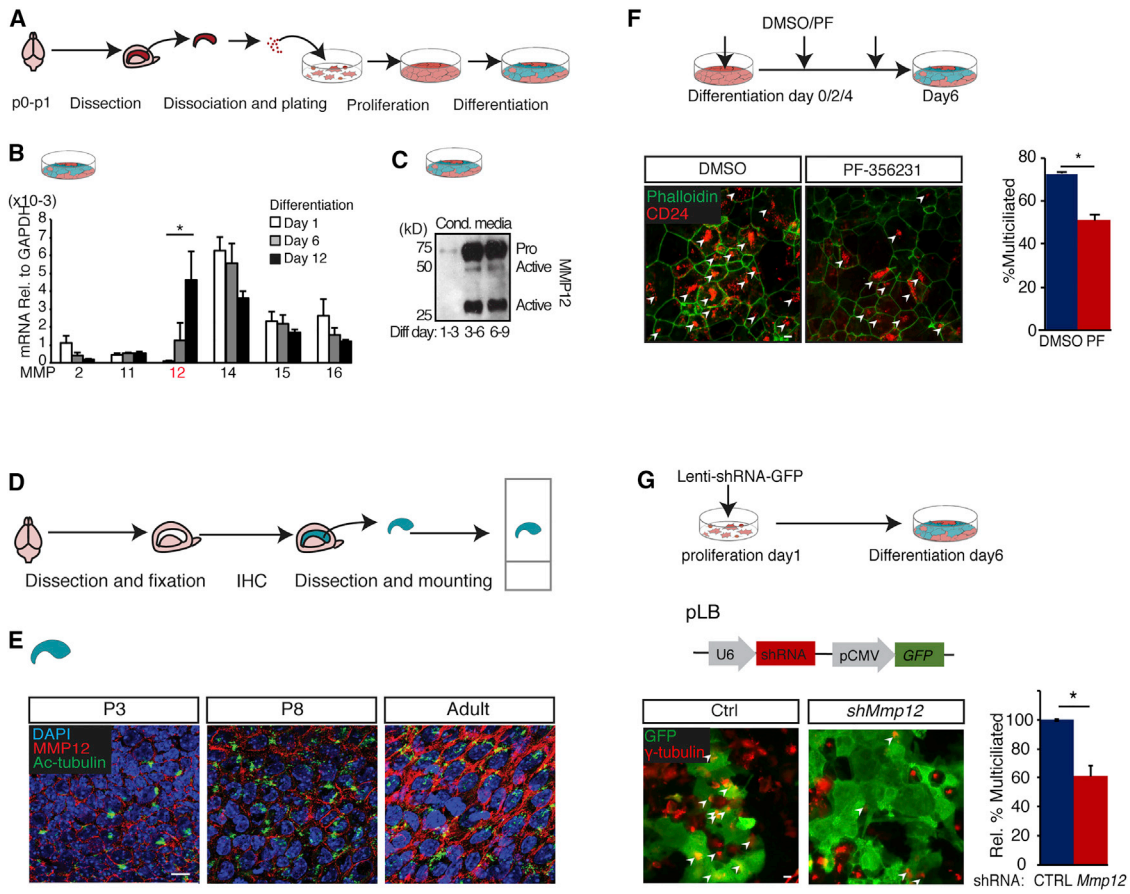

Figure 1. MMP Expression in the Developing V-SVZ Stem Cell Niche

(A) Schematic of ependymal cell (EC) cultures.

(B) Time course to assess mRNA levels of the most highly expressed *Mmp* family members in differentiating ECs reveals *Mmp12* is upregulated during differentiation (*$p < 0.05$, day 1 versus day 12, n = 3 independent experiments, one-way ANOVA with Tukey-Kramer correction).

(C) MMP12 western blotting of conditioned media from ECs at differentiation days 1–3, 3–6, and 6–9 (representative blot of 3 repeats).

(D) Schematic of V-SVZ whole-mount IHC.

(E) Representative images of V-SVZ whole-mount IHC at P3, P8, and P60 (adult). MMP12 is associated with multiciliated ECs (acetylated tubulin, Ac-tubulin), with MMP12 levels increasing during development.

(F) EC cultures treated with DMSO (vehicle) or PF-356231 (5 μM) at differentiation days 0, 2, and 4. The percentage of multiciliated ECs (CD24, EC marker co-localizing with cilia) is decreased by PF-356231 (arrowheads point to multiciliated ECs; error bars denote SEM; *$p < 0.05$, t test, n = 3 independent experiments).

(G) Upper: EC cultures were transduced with virus containing control shRNA (Ctrl) or *Mmp12* shRNA. Middle: lentiviral construct pLB. Lower: *Mmp12* shRNA significantly reduces the percentage of multiciliated ECs (arrowheads point to multiciliated GFP^+ cells; error bars denote SEM; *$p < 0.05$, t test, n = 3 independent experiments).

Scale bars, 10 μm.

of both extracellular and intracellular MMP12 during V-SVZ niche establishment. Our study reveals that extracellular MMP12 regulates the cellular and ECM rearrangements needed to build a mature niche, whereas intracellular MMP12 has a distinct function in regulating EC ciliogenesis, with both extracellular and intracellular MMP12 forms promoting NSC quiescence and thus regulating niche output.

RESULTS

Identifying MMP12 as a Possible Regulator of Postnatal V-SVZ Niche Development

To explore a potential role for MMPs in regulating V-SVZ niche development, we applied a broad-spectrum MMP inhibitor, GM6001, to V-SVZ EC cultures (see Figure 1A), and observed a significant block in EC maturation as judged by

the decrease in multiciliated (γ-tubulin$^+$) cells and *FoxJ1* promoter activity (Figures S1A and S1B). To determine the MMP(s) potentially responsible for this phenotype, we collected total mRNA from the EC cultures at days 1, 6, and 12 of differentiation and analyzed *Mmp* gene mRNA levels using qRT-PCR. Of the 24 *Mmps* and their splicing variants, only *Mmp2*, *11*, *12*, *14*, *15*, and *16* were highly expressed (>5 × 10^{-4} relative to *Gapdh*). Among these, *Mmp12* was unique in being strongly upregulated during EC differentiation (Table S1 and Figure 1B). We validated the presence of MMP12 protein, both pro- ($\geq$55 kDa) and active (22–45 kDa) forms, in western blots of conditioned media from differentiating ECs (Figure 1C). We next examined MMP12 *in vivo* using whole-mount immunohistochemistry (IHC) (Figure 1D), and identified MMP12 immunoreactivity associated with multiciliated ECs (visualized using acetylated α-tubulin immunoreactivity) that appeared to increase during V-SVZ niche development (Figure 1E).

To assess MMP12 function, we used a MMP12-specific inhibitor, PF-356231, and lentivirus-delivered *Mmp12* short hairpin RNA (shRNA), to specifically target MMP12 activity and expression in EC cultures (Figures 1F, 1G, S1C, and S1D for shRNA validation). The percentage of ECs that were multiciliated (CD24$^+$, with visible cilia patches) at day 6 was significantly decreased by 5 μM PF-356231 treatment (Figure 1F). Additional scoring of multiciliated ECs using γ-tubulin immunoreactivity resulted in a similar decrease in multiciliated cells by PF-356231 (vehicle: 53.4% ± 2.8%, n = 3; PF: 27.7% ± 4.2%, n = 3; p = 0.003). EC cultures were next transduced with lentivirus co-expressing shRNA and GFP (Figure 1G and Supplemental Experimental Procedures). Here, significantly fewer multiciliated ECs (γ-tubulin$^+$) were observed in lentivirus transduced cells (GFP$^+$) with *Mmp12* shRNA compared with control shRNA (Figure 1G).

A Functional Intracellular MMP12 Is Expressed in *Mmp12* Mutant Ependymal Cells

To further assess the function of MMP12 during V-SVZ niche development, we analyzed *Mmp12* mutant mice, B6.129X-*Mmp12*^{tm1Sds}/J (Shipley et al., 1996). However, using EC cultures prepared from *Mmp12* mutant mice, we noticed MMP12 immunoreactivity in cell cortices and nuclei that was similar to that in wild-type (WT) (Figure 2A). When examining the transgenic strategy of the *Mmp12* mutant, we noted that an in-frame start codon was preserved after replacing most of exon 2 with a flipped neomycin-STOP cassette (Figure 2B, mutant gene). If expressed, this gene product could produce a protein that lacks the signal peptide but preserves most of the catalytic domain and the hemopexin repeats, and would therefore be predicted to be a functional intracellular protein (Figure 2B, mutant protein).

While MMPs are conventionally known as extracellular proteins, intracellular functions were recently discovered in many MMPs (e.g., MMPs 2, 9, 12, and 14) (Houghton et al., 2009; Jobin et al., 2017; Lovett et al., 2012; Marchant et al., 2014; Shimizu-Hirota et al., 2012; Zhang et al., 2015). For MMP12 in particular, its hemopexin domain has been found to have an antibacterial function intracellularly in macrophages (Houghton et al., 2009). Furthermore, extracellular MMP12 was reported to be transported back into cells, where it enzymatically cleaves intracellular proteins as well as translocates into the nucleus and regulates transcription (Marchant et al., 2014). In addition, the NCBI Gene database describes two transcriptional variants of mouse *Mmp12* without a signal peptide sequence (NCBI Gene: NM_001320076.1, NM_001320077.1), based on RIKEN's functional annotation of the mammalian genome (e.g., Figure 2B, WT isoform 2). To date, the expression and function of these potential intracellular MMP12s remains uncharacterized. We used PCR primers targeting regions of the *Mmp12* gene that varied among *Mmp12* isoforms, and found a transcript consistent with *Mmp12* WT isoform 2, which is predicted to translate into an intracellular MMP12 (icMMP12, Figures S2A–S2D). To test whether a truncated, icMMP12-encoding mRNA is expressed in *Mmp12* mutant ECs, we used primers targeting different exons (Figure 2B, WT gene) to quantify *Mmp12* cDNA with qRT-PCR (Figure 2C). As expected exon 1-containing transcripts were significantly reduced in *Mmp12* mutant cells. In contrast, exons 4,5- and exons 7,8-containing transcripts were present in *Mmp12* mutant cells (and even upregulated compared with WT). The 5′ end of this potential mRNA in *Mmp12* mutant ECs was confirmed with 5′ RACE (rapid amplification of cDNA ends), with the predicted ATG being the only possible in-frame start codon (Figures S2E and S2F).

To determine whether icMMP12-encoding mRNA was translated into protein, we used cell lysates (to detect intracellular MMP12) and conditioned media (to detect extracellular MMP12) from WT and *Mmp12* mutant EC cultures for western blotting. Full-length MMP12 is a 55-kDa protein. Typically, the pro-domain at the N terminus is first cleaved off to generate a 45-kDa active enzyme, then processed on both N and C termini, producing several intermediate products as well as a mature 25-kDa protein, presumably consisting only of the catalytic domain (illustrated in Figure 2B) (Shapiro et al., 1992, 1993) (TopFIND: P34960). In WT cell lysates, we found that full-length MMP12 can be detected as a 45-kDa activated protein band, a few intermediate bands, and an ~25-kDa mature band, which is consistent with the known protein band pattern for MMP12 (Figure 2C). Furthermore, the >55-kDa species observed in conditioned media cannot be detected in cell lysates (for an example of an entire blot

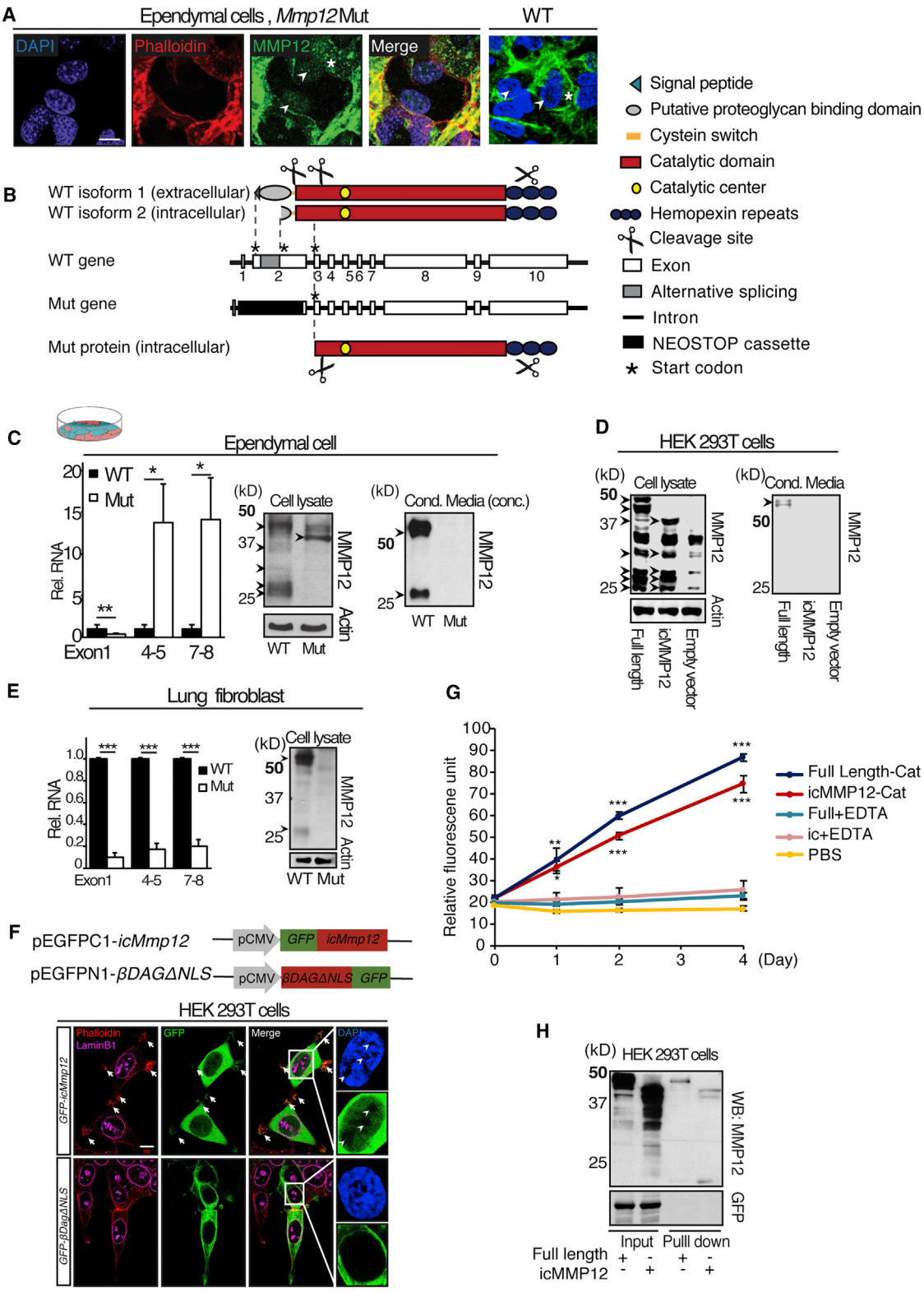

Figure 2. An Intracellular MMP12 Persists in *Mmp12* Mutant Ependymal Cells

(A) IHC of *Mmp12* mutant (Mut) and wild-type (WT) EC cultures at differentiation day 12, highlighting MMP12 in the cell cortex (asterisk, overlapping with phalloidin) and nucleus (arrowheads, DAPI).

(legend continued on next page)

see Figure S1C). On the other hand, in *Mmp12* mutant lysates, an ~40-kDa band was observed (Figure 2C), indicating the presence of the mutant icMMP12 predicted by mRNA analysis. Conditioned media from WT cells contained a >50-kDa band and an ~25-kDa band (Figure 2C). In contrast, the conditioned media from *Mmp12* mutant cells lack any detectable MMP12 (Figure 2C), consistent with a complete loss of secreted MMP12, as reported by Shipley et al. (1996).

To validate that the bands observed in *Mmp12* mutant lysates were indeed MMP12 proteins, we made expression constructs of full-length and truncated *Mmp12*, each preserving their native Kozak sequence. HEK293T cell lysates expressing the full-length or truncated recombinant MMP12s showed banding patterns similar to those of lysates from WT and *Mmp12* mutant EC cultures, respectively (Figure 2D, cell lysate). Consistent with EC cultures, only full-length *Mmp12* cDNA expressed secreted MMP12 (Figure 2D). Based on 5′ RACE (Figures S2E and S2F) and western blotting (Figures 2C and 2D), we inferred that translation of the icMMP12 in *Mmp12* mutant ECs starts from the predicted ATG site.

The B6.129X-*Mmp12*^{tm1Sds}/J mouse line had been used as a complete *Mmp12* knockout, with no intracellular MMP12 being reported (Houghton et al., 2009; Jobin et al., 2017; Shipley et al., 1996); therefore, we sought to determine whether mutant icMMP12 was found in other cells. In lung fibroblasts, which express high levels of MMP12, we found that, unlike ECs, all primer sets detected diminished levels of *Mmp12* cDNA in *Mmp12* mutant lung fibroblasts (Figure 2E). In WT lung fibroblasts the predominant MMP12 protein was ~55 kDa (Figure 2E), similar to what was detected in conditioned media from full-length *Mmp12* cDNA, with no detectable 40-kDa band as found in ECs (Figure 2C).

To assess mutant icMMP12 subcellular localization, we cloned *icMmp12* cDNA into pEGFP-C1 and transfected HEK293T cells (Figure 2F). GFP immunocytochemistry indicated that GFP-icMMP12 was cytosolic and nuclear. Nuclear icMMP12 co-localized with DAPI, consistent with previous observations that MMP12 can enter the nucleus and associate with DNA (Marchant et al., 2014). As a negative control, we transfected pEGFPN1-βDAGΔNLS whose protein product is excluded from the nucleus (Figure 2F). We also transfected GFP-icMMP12 into both the V-SVZ (using neonatal ventricle electroporation) and EC cultures, and detected nuclear immunoreactivity in V-SVZ cells (Figures S2G and S2H).

Given that the mutant icMMP12 catalytic domain is slightly truncated, we wanted to confirm its biological activities. To test for enzymatic activity, we transfected 293T cells with full-length or icMMP12 catalytic domain tethered with a C-terminal 7xHis tag (pCDNA3.1^{+}-*FLMmp12*Cat-7His, pCDNA3.1^{+}-*icMmp12*Cat-7His) and prepared recombinant protein with Ni-nitrilotriacetic acid agarose beads under native conditions. Using an MMP12-specific enzymatic activity assay, full-length MMP12 and icMMP12 were both found to be enzymatically active (Figure 2G). Streptavidin-agarose pull-down assays were performed to assess DNA-binding ability (Figure 2H). After co-transfecting HEK293T cells with pEF1-mmp12-V5His and pMAX-GFP, or, with pEF1-icmmp12-V5His and pMAX-GFP, we incubated cell lysates with a 5′-biotinylated DNA oligo described to bind to

(B) *Mmp12* gene and MMP12 protein domains in WT and Mut mice. Splicing variations in exon2 lead to alternative *Mmp12* transcripts in WT cells (WT isoform 2).

(C) MMP12 expression in WT and Mut ECs. Left: qPCR analysis with primers targeting different *Mmp12* exons. Note the high levels of *Mmp12* mRNA in Mut ECs only from primers targeting downstream exons (WT, n = 5; Mut, n = 6; 5 independent experiments; *p < 0.05, **p < 0.01, t test). Middle: western blots of cell lysates to detect intracellular MMP12 (icMMP12). An ~40-kDa band is detected in Mut. Right: western blots of conditioned media to detect extracellular MMP12. No MMP12 is detected in Mut.

(D) Western blots of HEK293T cells transfected with constructs containing full-length or icMMP12 cDNA. Left: cell lysates. Right: conditioned media. Note that full-length and icMMP12 show similar patterns (arrowheads) as WT and Mut, respectively, in (C).

(E) MMP12 expression in WT and Mut lung fibroblast cells. Left: qRT-PCR. *Mmp12* transcript is diminished at all tested exons (n = 3 independent experiments, ***p < 0.001, t test). Right: western blots of cell lysates. No 40-kDa band is detected in Mut, as compared with (C).

(F) Confocal images of GFP IHC in HEK293T cells transfected with GFP-icMMP12 or βDAGΔNLS-EGFP. In contrast to βDAGΔNLS-EGFP, GFP-icMMP12 co-localizes with DAPI-stained nuclear DNA. Arrowheads indicate that DAPI^{-} areas are also negative for GFP-icMMP12. GFP-icMMP12 also co-localizes with phalloidin at filopodia (arrows).

(G) MMP12 enzymatic activity assay on purified full-length or mutant icMMP12 catalytic domain proteins. Both proteins when incubated with FRET peptide substrate upregulated 480/530 nm fluorescent signal, compared with 50 mM EDTA-treated negative control or PBS (full-length catalytic domain, n = 3; icMMP12 catalytic domain, n = 4; full-length or icMMP12 + EDTA, n = 3; PBS, n = 5; 3 independent experiments, one-way ANOVA with Tukey-Kramer correction; *p < 0.05, **p < 0.01, ***p < 0.001).

(H) Streptavidin-agarose pull-down assay on HEK293T cells transfected with full-length MMP12 and icMMP12. Both full-length-MMP12 and icMMP12 were pulled down with a 5′ biotinylated DNA 50mer known to bind MMP12 (representative blot for 3 independent experiments). Error bars denote SEM. Scale bars, 10 μm.

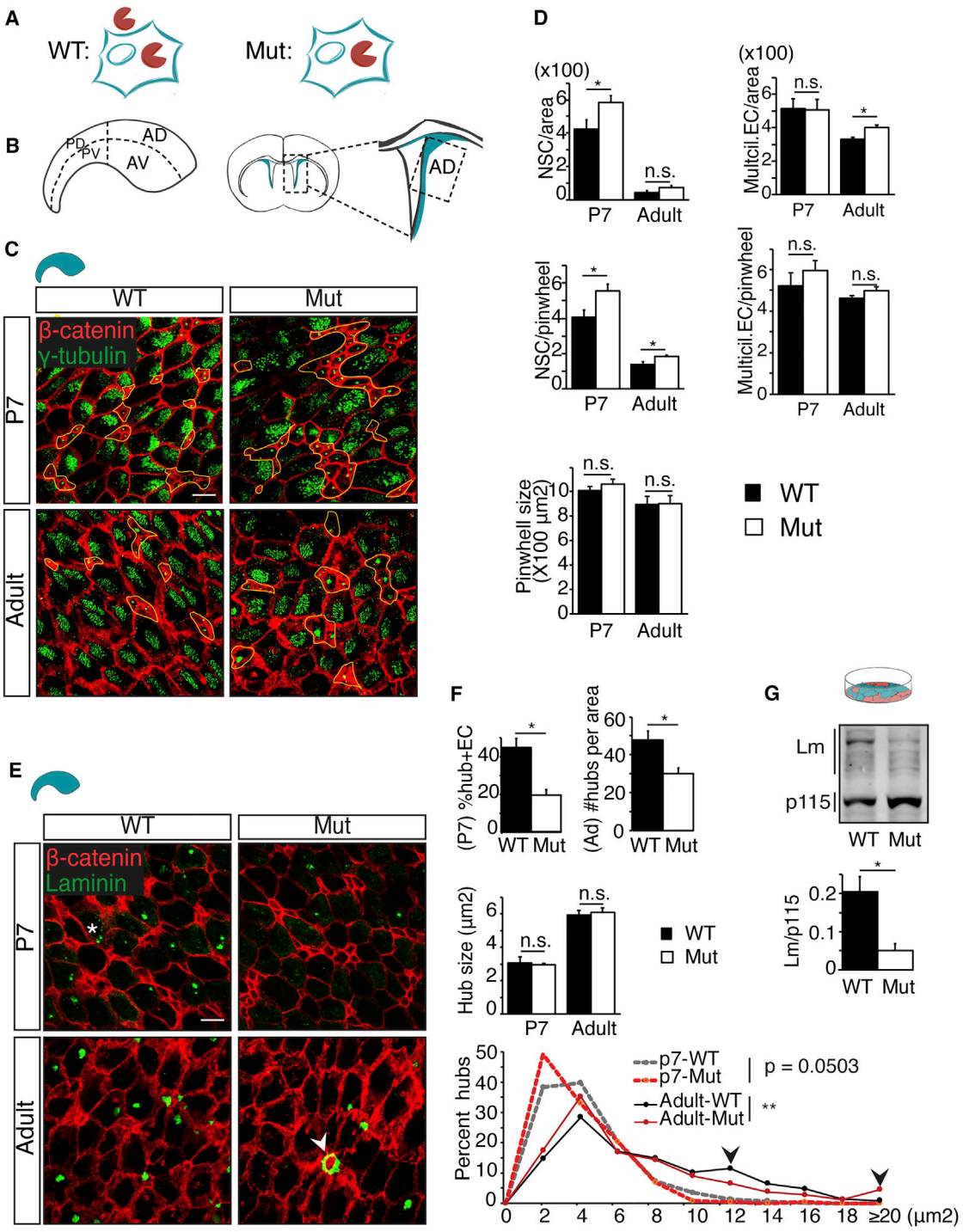

Figure 3. Extracellular MMP12 Regulates V-SVZ Niche Cellular and ECM Organization

(A) The presence or absence of extracellular and intracellular MMP12s in WT and *Mmp12* mutant (Mut) cells.

(B) V-SVZ areas analyzed in this study. Left: whole-mount V-SVZ. Right: an anterior brain coronal section. AD, anterior dorsal; AV, anterior ventral; PD, posterior dorsal; PV, posterior ventral.

(C) Representative images of WT and Mut whole-mount IHC to indicate cell junctions (β-catenin) and ciliary basal bodies (γ-tubulin). Neural stem cell (NSC) clusters are highlighted in yellow.

(legend continued on next page)

MMP12 (Marchant et al., 2014). Streptavidin-agarose beads pulled down both full-length (45 kDa) and icMMP12 (40 kDa), but not co-transfected GFP, suggesting that icMMP12 retains DNA-binding activity.

Extracellular MMP12 Regulates V-SVZ Neural Stem Cell Niche Pinwheel Organization

Given that *Mmp12* mutant ECs retain a functional icMMP12, we were able to use this mouse to explore the functions of extracellular MMP12 in postnatal V-SVZ development (Figure 3A). We focused our analysis within the anterior-dorsal V-SVZ as it contains the most typical ECs and pinwheels (Figure 3B), performing whole-mount IHC on WT and *Mmp12* mutant mice with β-catenin antibodies to label cell junctions and γ-tubulin antibodies to label ciliary basal bodies (Figure 3C). NSCs were defined by their small apical surface area and single cilium basal body, and ECs by their larger apical surface area and patches of ciliary basal bodies. At postnatal day 7 (P7) the *Mmp12* mutant V-SVZ had more NSCs per area than in WT (Figure 3D, top left), as well as more NSCs per pinwheel in P7 and adult (8-week) mice, although overall pinwheel sizes were not affected (Figure 3D, middle and bottom). In contrast, the adult *Mmp12* mutant V-SVZ contained slightly more ECs (Figure 3D, top right), although the number of ECs per pinwheel were not significantly affected (Figure 3D, middle right). Considering V-SVZ regional heterogeneities, we also examined the anterior-ventral (AV) and posterior-dorsal (PD) V-SVZ, areas known to contain niche pinwheels (Shook et al., 2012). We found similar increases in NSCs per pinwheel and NSCs per area in the AV, but not PD, V-SVZ (Figures S3A and S3B). Together, these results indicate that the lack of *extracellular* MMP12 leads to disturbances in V-SVZ niche pinwheel organization in the anterior V-SVZ, although EC maturation appears to proceed with relative normality.

To determine whether extracellular MMP12-regulated ECM hubs, aggregated ECM structures near the ventricle surface (McClenahan et al., 2016), we performed whole-mount IHC with a polyclonal laminin-111 antibody that detects the majority of laminin subtypes. At P7 ECM hubs were not fully formed, so we measured the percentage of ECs with ECM aggregates (Figure 3E, asterisk), while in the adult V-SVZ we assessed ECM hub density and ECM hub size. We found that *Mmp12* mutants had significantly fewer ECM-associated ECs at P7 and fewer ECM hubs per area in adulthood (Figure 3F, top). Although the mean ECM hub sizes were similar in WT and *Mmp12* mutant (Figure 3F, middle), ECM hubs in *Mmp12* mutants had altered size distributions, with fewer medium-sized hubs and more abnormally large ones (Figure 3E, arrowhead; Figure 3F, bottom, arrowheads). *Mmp12* mutant EC cultures had less laminin protein (Figure 3G); however, no obvious changes in laminin cleavage products were observed in cell lysates (not shown). Together these data indicate an aberrant V-SVZ ECM in mice that lack extracellular MMP12.

Since laminin can be a substrate of MMP12, it was surprising that eliminating extracellular MMP12 would lead to *less* laminin. As all laminin subunit mRNA transcripts were at normal levels in *Mmp12* mutant ECs (not shown), MMP12 likely regulates laminin at the post-transcriptional level. One possibility is an upregulation of other MMPs or downregulation of TIMPs (tissue inhibitors of metalloproteinases), leading to enhanced laminin digestion. Out of all the *Mmps* and *Timps*, we found that only *Mmp2* mRNA levels were modestly upregulated in *Mmp12* mutant EC cultures (Figures S4A and S4C). However, we detected similar levels of the MMP2 pro-enzyme and no activated MMP2 protein from either WT or *Mmp12* mutant cells by gelatin zymography (Figure S4B) We also found no change in protein levels of β-dystroglycan and α6-integrin, two laminin receptors whose loss could affect cell association with laminin, and no change in mRNA levels of β1 and β4, the integrin β subunits that associate with α6 (Figure S4D).

Extracellular MMP12 Regulates Translational Planar Cell Polarity of V-SVZ ECs

To determine whether extracellular MMP12 regulates V-SVZ translational planar cell polarity, we analyzed whole mounts for basal body patch displacement and angle distribution (Figure 4A), as described by Mirzadeh et al. (2010b). We found that V-SVZ translational polarity was disturbed in both P7 (Figures 4B and 4D [left]) and adult *Mmp12*

(D) Quantification of NSCs, ECs, and pinwheels. NSCs/area at P7, multiciliated ECs/area at adult, and NSCs/pinwheel at P7 and adult are increased in Mut (P7 WT, n = 6 mice; P7 Mut, n = 6 mice; adult WT, n = 4 mice; adult Mut, n = 3 mice; *p < 0.05, t test).
(E) Representative images of WT and Mut whole-mount IHC to indicate cell junctions (β-catenin) and ECM hubs (laminin). Adult ECM hubs are often abnormal in size in Mut (arrowheads) (*p < 0.05, t test).
(F) The percentage of ECs with ECM at P7 and the ECM hubs per area in adults are both lower in Mut V-SVZ (*p < 0.05, t test; P7 WT, n = 4 mice; Mut, n = 4 mice; adult WT, n = 5 mice; Mut, n = 6 mice). In adults, Mut hub size distribution is different than in WT (**p < 0.01 by Kolmogorov-Smirnov test; P7 WT, n = 674 hubs; Mut, n = 273, from 4 mice each; adult WT, n = 883, 5 mice; Mut, n = 587, 6 mice).
(G) Mut EC cultures at differentiation day 12 have a significantly lower level of laminin (WT, n = 4; Mut, n = 3; 3 independent experiments; *p < 0.05, t test).
Error bars denote SEM. Scale bars, 10 μm.

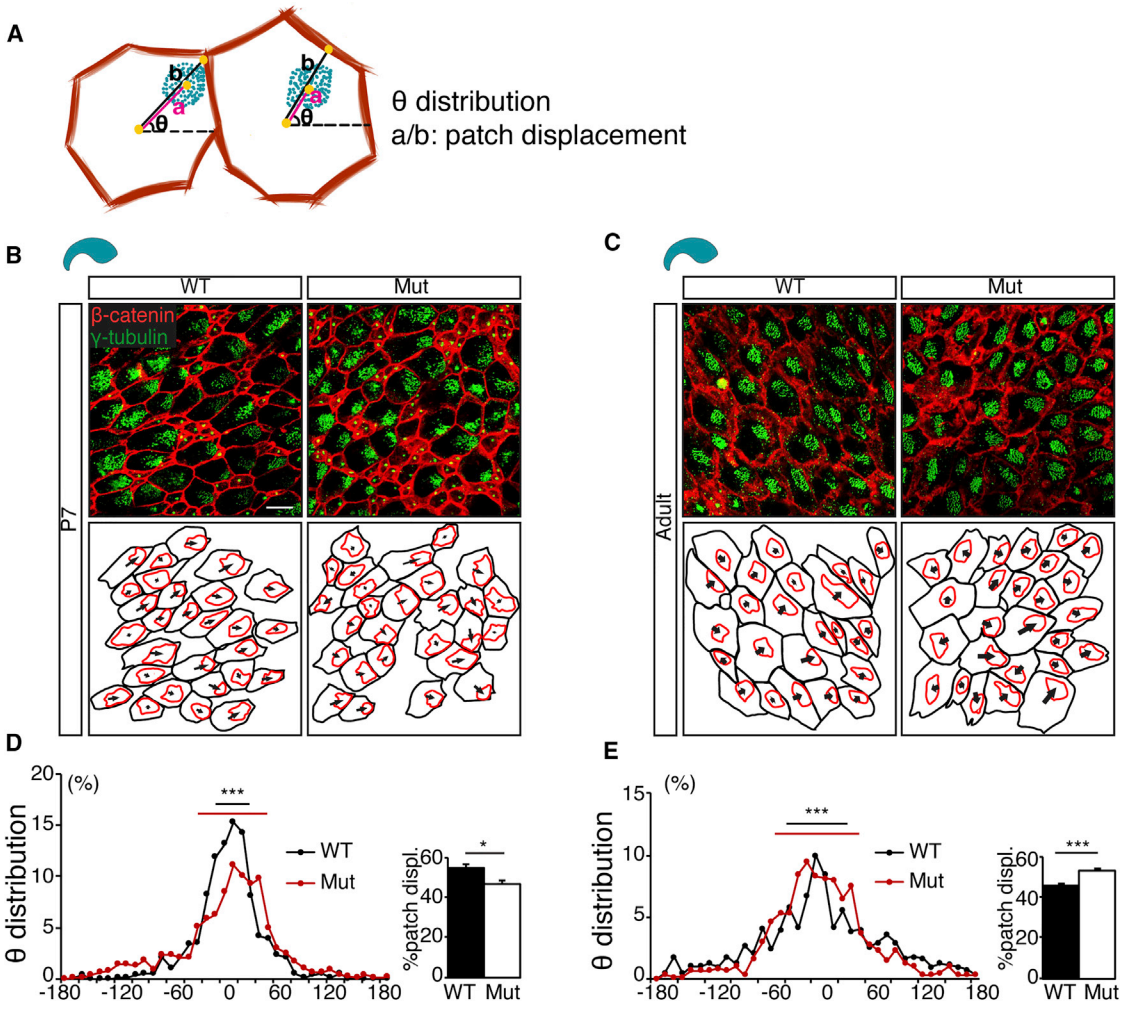

Figure 4. Extracellular MMP12 Regulates EC Translational Planar Cell Polarity

(A) Planar cell polarity analysis. Cell boundaries (red) and ciliary basal body (green) patches were traced to calculate their respective centers (yellow). The distance between the centers (a) and distance between cell center and cell border (b) are used to calculate basal body patch displacement (a/b). The distribution of line angles (θ) throughout the field was measured.

(B and C) Representative images of WT and *Mmp12* mutant (Mut) whole-mount IHC (upper) and tracings (lower) at P7 (B) and adult (C). Arrows indicate displacement of basal body patches from cell centers.

(D and E) Quantification of θ distribution and patch displacement. θ distributions are disrupted in Mut at P7 and adult (***$p < 0.001$, Watson's U^2). Mut patch displacements are decreased at P7 (*$p < 0.05$, t test) and increased in adults (***$p < 0.001$, t test). Four or more mice were analyzed in each group. Cells traced: P7 WT, n = 571 cells; P7 Mut, n = 1,354; adult WT, n = 960; adult Mut, n = 814. Error bars denote SEM. Scale bars, 10 μm.

mutant mice (Figures 4C and 4E [left]). Basal body patches were less displaced in *Mmp12* mutants at P7 (Figure 4D, right), indicative of decreased EC maturity, but more displaced in adults (Figure 4E, right). The abnormality in patch displacement was not a result of alterations of basal body patch sizes (P7: WT = 29.61 ± 1.45 μm^2, n = 4 mice; Mut = 30.54 ± 1.76 μm^2, n = 5; p = 0.68; adult: WT = 35.47 ± 1.59 μm^2, n = 4; Mut = 33.26 ± 0.57 μm^2, n = 3; p = 0.30). The AV and PD V-SVZ of P7 *Mmp12* mutant mice also had dispersed patch angle distributions, but no significant changes in patch displacement (Figure S3C).

Intracellular MMP12 Promotes Ependymal Ciliogenesis via FOXJ1

In contrast to MMP12 pharmacological inhibition or *Mmp12* shRNA knockdown with which EC ciliogenesis was inhibited (Figures 1F and 1G), *Mmp12* mutant mice, which serve as an extracellular MMP12 knockout, had

normal EC ciliogenesis both *in vivo* (Figures 3C and 3D) and *in vitro* (not shown). Because the MMP12 inhibitor PF-356231 and *Mmp12* shRNA are predicted to suppress both extracellular and intracellular MMP12, we hypothesized that the ciliogenic defects in these experiments could reflect separate functions of intracellular MMP12 (icMMP12). To manipulate potential icMMP12 expression in the developing V-SVZ, we used neonatal ventricle electroporation to introduce plasmids to the V-SVZ at P1 followed by an analysis of EC ciliogenesis (Figure 5A). First, we electroporated both WT and *Mmp12* mutant mice with an *Mmp12* shRNA plasmid co-expressing histone H2B-CFP (pH2B-CFP-SUPER), then analyzed V-SVZ whole mounts at P7 (Figure 5B). In WT mice, *Mmp12* shRNA prevents both extracellular and intracellular MMP12 expression, whereas in *Mmp12* mutant mice, *Mmp12* shRNA prevents icMMP12 expression in cells that already lack extracellular MMP12, therefore revealing potential functions of icMMP12 (Figure 5C, schematics). *Mmp12* shRNA reduced the percentage of multiciliated cells that emerged from transfected CFP$^+$ VZ cells in both WT and *Mmp12* mutant mice (Figure 5C). We also found no cleaved-caspase-3$^+$ cells in the EC layer, indicating that cell death is unlikely to be contributing to the decrease in mature ECs (Figure S5A). If icMMP12 is required for ciliogenesis, then a prediction is that overexpressing icMMP12 may promote ciliogenesis. We therefore electroporated an icMMP12 construct into P1 WT mice (Figure 5D), and evaluated the whole mount at P5 to better catch a potential enhancement of EC ciliogenesis. Indeed, icMMP12 overexpression increased the percentage of multiciliated ECs that formed by P5 (Figure 5E). To determine whether icMMP12 affected ECM hub formation, we overexpressed icMMP12 in WT neonates through ventricle electroporation and analyzed whole mounts using laminin IHC. However, we did not observe significant changes in the percentage of ECM hub$^+$ cells on the ventricular surface (control, 7.8% ± 1.1%, n = 5; icMMP12, 10.6% ± 1.8%, n = 4, p = 0.21), which suggests that icMMP12 is not instrumental for ECM hub formation.

FOXJ1 has been shown to be a master regulator of ciliogenesis in ECs as well as in other multiciliated cells (Jacquet et al., 2009). As GM6001 (a pan-MMP inhibitor) blocked *FoxJ1* transcription in EC cultures (Figures S1A and S1B), we hypothesized that icMMP12 may support ciliogenesis by regulating FOXJ1 levels. To test this, we electroporated *Mmp12* mutant mice at P1 with control or *Mmp12* shRNA, as above (Figure 5B), and analyzed whole mounts at P7 to determine the percentage of FOXJ1$^+$ cells within the CFP$^+$ cells. We found that *Mmp12* shRNA on the background of *Mmp12* mutant mice significantly decreased the percentage of FOXJ1$^+$ cells, indicating that icMMP12 regulates EC ciliogenesis at the level of, or upstream of, FOXJ1 (Figure 5F).

Extracellular and Intracellular MMP12 Both Promote Neural Stem Cell Quiescence

To investigate potential roles for extracellular and intracellular MMP12 in niche function, we analyzed the proliferation of NSCs (SOX2$^+$MASH1$^-$) and transient amplifying progenitors (TAPs, SOX2$^+$Mash1$^+$) in the *Mmp12* mutant and WT littermate V-SVZ (Figure 6A), as well as in the mmp12 mutant V-SVZ following either *Mmp12* or control shRNA (Figure 6E). Coronal sections were assessed by IHC for Ki67 to detect proliferating cells, and SOX2 to detect a combination of NSCs and TAPs. At P7, V-SVZ in *Mmp12* mutant mice had a higher percentage of proliferating SOX2$^+$ cells than WT mice (Figures 6A and 6D [left]). shRNA-mediated loss of icMMP12 in the *Mmp12* mutant V-SVZ also increased proliferation (Figures 6E and 6H [left]). To distinguish NSCs and TAPs within the SOX2$^+$ cell pool, we co-labeled Mash1, a TAP marker (Lee et al., 2012), and Ki67, and found no changes in proliferative TAPs (Figures 6B, 6D [middle], 6F, and 6H [middle]). Finally, considering that >90% of TAPs were proliferative, a shift in the %TAPs within the total SOX2$^+$ pool could also contribute to the increase in SOX2$^+$ cell proliferation. However, we found no change in the %Mash1$^+$ out of the total SOX2$^+$ cell pool (right-hand panels of Figures 6C, 6D, 6G, and 6H), indicating that the increase in proliferation in SOX2$^+$ cells reflects increased NSC activation.

Mmp12 mutant mice (lacking extracellular MMP12) were previously reported to have delayed myelination in the absence of any change in oligodendrocyte progenitors (Larsen et al., 2006), but it remained unclear whether icMMP12 influences neurogenesis and oligodendrogenesis. We therefore introduced *Mmp12* shRNA by ventricle electroporation into *Mmp12* mutant mice and assessed neuronal (DCX$^+$) and oligodendroglial (OLIG2$^+$) progenitors in whole mounts. The fractions of neuronal and oligodendroglial progenitors were similar to those of *Mmp12* and control shRNAs (Figure S5B) suggesting that icMMP12 does not affect NSC fate decisions. To determine whether MMP12 influenced rostral migration of neuroblasts, we compared the olfactory bulb (OB) in WT and *Mmp12* mutants or performed icMMP12 knockdown in the *Mmp12* mutant V-SVZ. After electroporating constructs at P1 and assessing coronal sections at P7 (Figure S5C), we found more H2B-CFP$^+$ cells in the OB when icMMP12 was silenced (Figures S5C–S5F), indicating that icMMP12 may influence the ability of V-SVZ neuroblasts to reach their OB target.

DISCUSSION

We investigated the potential role of the MMP family in the development of the V-SVZ NSC niche and found that

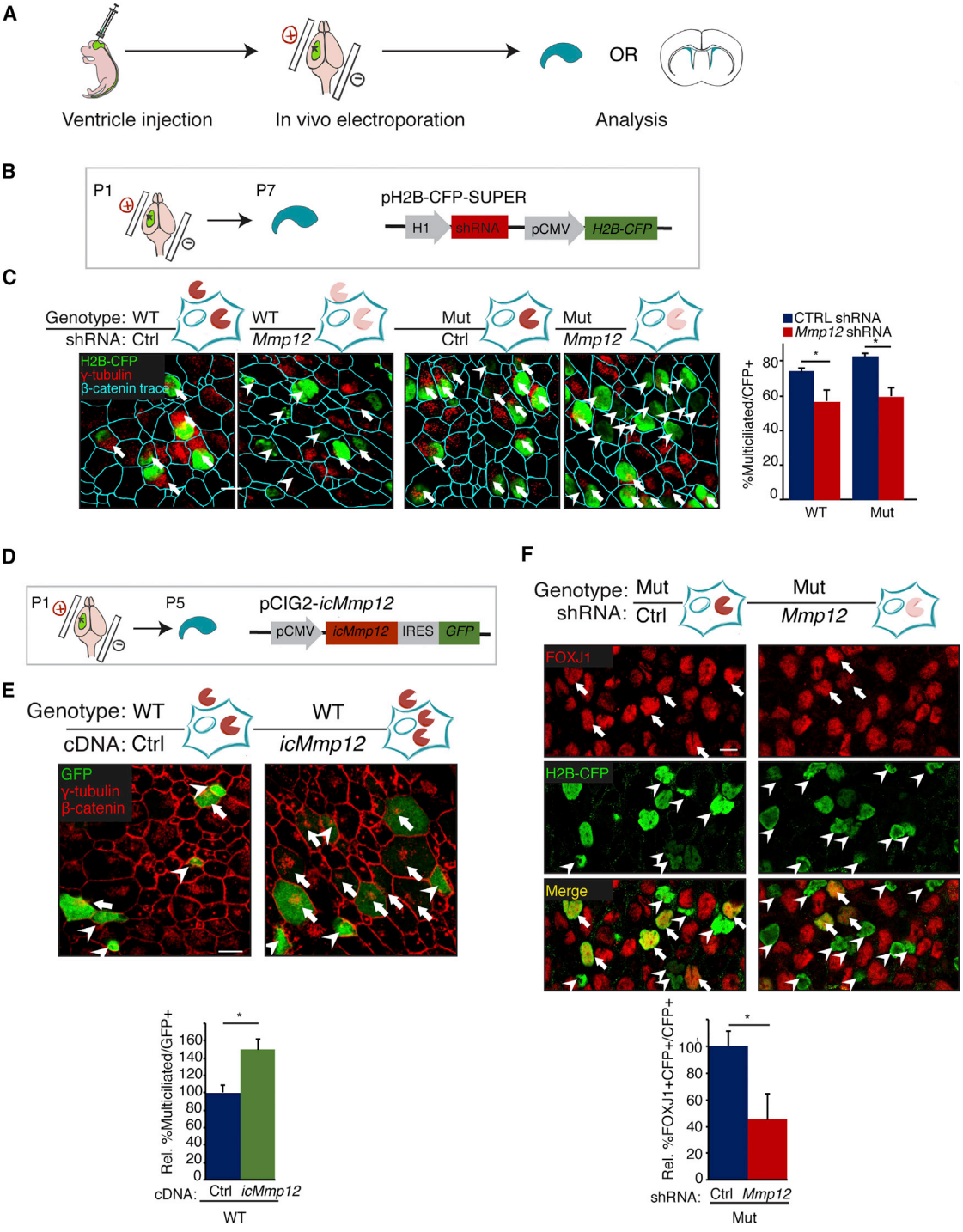

Figure 5. Intracellular MMP12 Regulates EC Ciliogenesis

(A) Schematic of neonatal *in vivo* electroporation.

(B) *In vivo* electroporation of WT and *Mmp12* mutant (Mut) mice with scrambled shRNA or *Mmp12* shRNA.

(C) Left: representative images of whole-mount IHC at P7. Arrows, multiciliated H2B-CFP$^+$ cells. Arrowheads, non-multiciliated H2B-CFP$^+$ cells. Right: in both WT and Mut mice, *Mmp12* shRNA significantly reduced the percentage of multiciliated H2B-CFP$^+$ cells (WT, n = 4 mice; Mut, n = 3 mice; *p < 0.05, t test).

(D) *In vivo* electroporation of WT mice with *icMmp12* cDNA co-expressing GFP, followed by whole-mount IHC at P5.

(legend continued on next page)

MMP12 is not only highly expressed in developing ECs but regulates EC maturation and, ultimately, V-SVZ niche output. While MMPs have been found to regulate other stem cell niches (Heissig et al., 2002; Kessenbrock et al., 2013; Nishida et al., 2012), in the V-SVZ only one other MMP, MMP24 (MT5-MMP), has been linked to V-SVZ stem cell niche function, where it is enriched in adult NSC cell junctions and has been shown to regulate adult V-SVZ stem cell quiescence (Porlan et al., 2014). Since it is currently unknown whether *Mmp24* plays a role in the development of the V-SVZ NSC niche, our finding that MMP12 regulates EC and V-SVZ niche development is the first to report this role for any MMP.

Surprisingly, we found that *Mmp12* mutant ECs express a truncated yet functional intracellular MMP12 protein, which we referred to as icMMP12, whose expression may be cell type specific. We further found that the loss of the extracellular MMP12 had no effect on EC ciliogenesis, while the loss of icMMP12 attenuated EC ciliogenesis, demonstrating that icMMP12 is sufficient to support MMP12's role in EC ciliogenesis. Although MMPs are well known as extracellular proteases, a recent landmark study has suggested that extracellular MMP12 can be taken up by cells and then function intracellularly, both as a protease and as a transcriptional regulator (Marchant et al., 2014). In addition, two variant transcripts have been predicted to produce an intracellular-only MMP12. Indeed, we found that one of these alternative transcripts is likely to be present in WT ECs. Therefore ECs may contain a unique pool of MMP12 whose sole function is intracellular. A better understanding of the expression patterns of the different *Mmp12* isoforms, both developmentally and across different cell types, may help to reveal new insights into the putative roles of intracellular MMP12.

The distinct cellular locations of extracellular and intracellular MMP12s indicated that they may have unique functions. By comparing the V-SVZ in WT and *Mmp12* mutant mice, which solely lack the secreted, extracellular MMP12, we concluded that extracellular MMP12 regulates the development of the V-SVZ niche pinwheel organization and associated ECM. Since a main function of MMPs is as a protease that can cleave the ECM, it was surprising that *Mmp12* mutant mice had *fewer* ECM hubs and *decreased* laminin levels, in contrast to the laminin *accumulation* in alveoli previously reported in *Mmp12* mutant mice (Warner et al., 2004). This indicates that the ECM disturbances in the V-SVZ of *Mmp12* mutant mice likely do not occur directly through altered laminin degradation by MMP12. We therefore explored the possibility that alterations in other MMPs, TIMPs, α6-containing integrins, or dystroglycan may lead to the ECM phenotypes, but found no obvious differences. This does not eliminate the possibility that other MMPs and proteases may be responsible for the altered ECM and cellular arrangements found in the *Mmp12* mutant V-SVZ, which could occur via changes in their translation, secretion, or activation state.

ECM hubs first appear in the V-SVZ at P6–P7 on surfaces of ECs and are thought to be important for regulating niche NSCs by capturing growth factors found in the CSF (Mercier, 2016). ECM hubs are thought to be anchored by integrin and dystroglycan ECM receptors, which may serve to initiate signaling cascades influential to NSC behavior (McClenahan et al., 2016; Shen et al., 2008). While the mechanism by which ECM hubs are produced and organized remains unknown, possible mechanisms include spatially targeted ECM deposition or clearance, or aggregating/relocating existing ECM. While ECM hubs appear to form while associated with ECs, VZ microglia may also contribute to hub development, as VZ microglia express several ECM proteins and proteases including MMP12 (Shigemoto-Mogami et al., 2014). The discovery that MMP12 regulates VZ ECM hubs may help to shed light on the mechanism(s) by which ECM hub development proceeds.

While *Mmp12* mutant mice have disturbances in the translational planar cell polarity of VZ ECs, ciliogenesis itself remained unchanged. Yet, surprisingly, inhibiting MMP12 activity with a membrane permeable compound caused ciliogenic defects in EC cultures, suggesting that icMMP12 is involved in ciliogenesis. We performed shRNA knockdown or overexpression of icmmp12 *in vivo* to test this hypothesis, and furthermore found that icMMP12 regulates EC ciliogenesis through FOXJ1, a transcription factor required for multiciliogenesis (Jacquet et al., 2009). As MMP12 has been reported to act both as an intracellular protease and transcription regulator, it will be interesting to determine whether icMMP12 regulates FOXJ1 levels through its proteolytic activities or through a transcriptional-modulatory mechanism.

Stem cell niches and their support cells tightly control stem cell behaviors (Li and Xie, 2005). In the current study, we found that either selective loss of extracellular MMP12 (comparing WT with *Mmp12* mutants) or loss of icMMP12

(E) Representative IHC images at P5. Arrows, multiciliated GFP^+ cells. Arrowheads, non-multiciliated GFP^+ cells. The relative percentage of multiciliated GFP^+ cells was increased by icMMP12 overexpression (Ctrl, n = 5 mice; *icMmp12*, n = 6 mice; $^*p < 0.05$, t test).
(F) Same experimental scheme as in (B). Upper: Representative images of FOXJ1, GFP co-IHC (arrows, $FOXJ1^+CFP^+$ cells; arrowheads, $FOXJ1^-CFP^+$ cells). Lower: The percentage of $FOXJ1^+$ cells within the CFP^+ cell population was decreased by *Mmp12* shRNA (ctrl shRNA, n = 5 mice; *Mmp12* shRNA, n = 4 mice; $^*p < 0.05$, t test).
Error bars denote SEM. Scale bars, 10 μm.

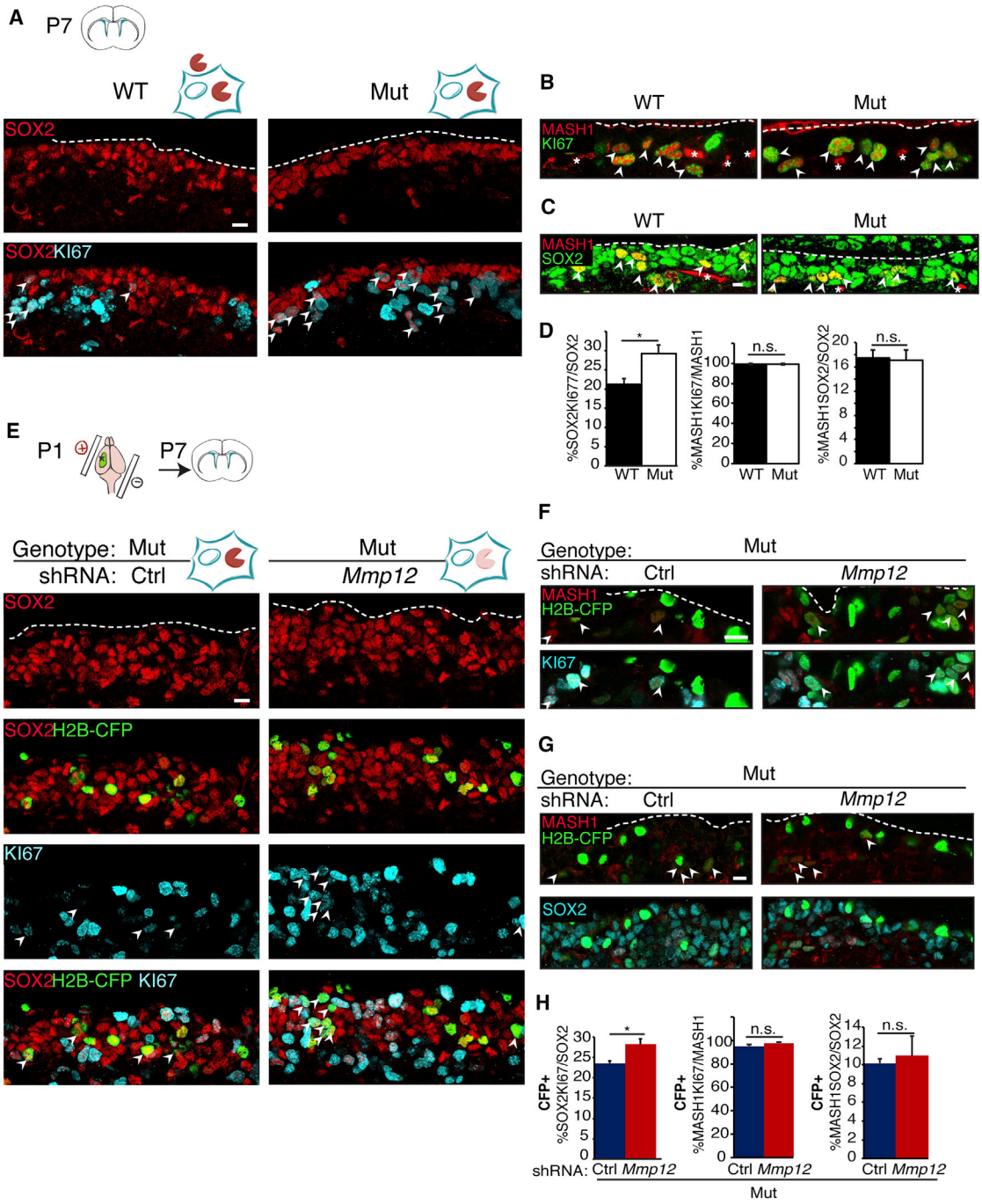

Figure 6. Extracellular and Intracellular MMP12 Both Suppress NSC Proliferation

(A–C) IHC in coronal sections from WT and *Mmp12* mutant (Mut) mice at P7. Arrowheads, double-positive cells; asterisks, non-specific vascular staining.

(D) Quantification of (A), (B), and (C) (left to right). The %Ki67$^+$ cells within the SOX2$^+$ cell population is significantly increased in Mut (WT, n = 6 animals; Mut, n = 9; *p < 0.05, t test). The %Ki67$^+$ cells within MASH1$^+$ cells, or the %MASH1$^+$ cells within SOX2$^+$ cells are not changed (WT, n = 4 mice; Mut, n = 4 mice; p > 0.05, t test).

(E–G) IHC in coronal sections from P7 Mut mice electroporated with control (Ctrl) or *Mmp12* shRNA. (E) SOX2, H2B-CFP, Ki67 co-IHC. (F) MASH1, H2B-CFP, Ki67 co-IHC. (G) MASH1, H2B-CFP, SOX2 co-IHC. Arrowheads point to triple-positive cells.

(legend continued on next page)

via knockdown strategies led to a significant upregulation of NSC proliferation. As *Mmp12* mRNA was virtually non-detectable in NSCs *in vitro*, we inferred that enhanced NSC proliferation in response to MMP12 loss was most likely an indirect consequence of disturbed niche support cells. For example, secreted MMP12 originating from ECs may normally influence surface proteins on NSCs, or translocate into NSCs to regulate NSC activation state. Consequently, loss of extracellular MMP12, originating from ECs, could affect NSC proliferation by disturbing NSC-intrinsic mechanisms. On the other hand, changes in NSC proliferation seen following the loss icMMP12 in the *Mmp12* mutant V-SVZ, may occur due to dysregulated timing of EC differentiation that in conjunction alters the activation dynamics of the postnatal NSC pool. Recent evidence indicates that adult neurogenesis is important in neuron-circuit plasticity (Obernier et al., 2014) and is required for olfactory-dependent behaviors (Gheusi et al., 2000; Sakamoto et al., 2011). As increased NSC proliferation may lead to early depletion of the NSC pool, it will be important to investigate how MMP12 can affect the aging V-SVZ and related neuron-circuit homeostasis.

The early postnatal V-SVZ undergoes complex organizational changes in a short span of time to generate the adult NSC niche, in a process that is only partly understood. This study demonstrates that MMP12 is involved in multiple aspects of V-SVZ niche development, leading to changes in this stem cell niche's function, and additionally reveals a unique function of intracellular MMP12 in EC maturation. These discoveries provide new insight into how MMPs can act to sculpt both the form and function of developing stem cell niches, with implications for homeostasis in adult and aging brains.

EXPERIMENTAL PROCEDURES

Animals

Mice were housed and cared for according to NIH and IACUC guidelines. C57/bl6 mice and mutant mice of C57/bl6 background (B6.129X-*Mmp12*^{tm1Sds}/J) (Shipley et al., 1996) were from The Jackson Laboratory. *FoxJ1*-promoter GFP-transgenic mice were a gift from Dr. Ken-Ichi Takemaru (Ostrowski et al., 2003).

Image Acquisition and Analysis

Confocal images were acquired from Zeiss LSM510 or LeicaSP8X confocal laser-scanning microscopes. Selected fluorescent images for cell culture were acquired using a Zeiss Axiovert 200M epifluorescent microscope. Image analysis was done with Fiji software, and data processing for planar cell polarity was done with MATLAB software (Supplemental Experimental Procedures).

Statistical Analysis

Statistical analyses (one-way ANOVA followed by multiple comparisons with Tukey-Kramer corrections, Watson's U^2, and Kolmogorov-Smirnov test) were performed using MATLAB. t Tests were performed with Excel. $p < 0.05$ was considered statistically significant.

Antibodies and Dyes

Please refer to Supplemental Experimental Procedures for full details.

Primers, DNA Oligos, and Sequencing

DNA sequencing was carried out at Stony Brook Genomics Core Facility. Please refer to Supplemental Experimental Procedures for a list of primers.

MMP12 Enzymatic Activity Assay

Proteolytic activity of MMP12 was analyzed with SensoLyte 520 MMP-12 assay kit. Sodium azide (0.02%) was added to all reactions to prevent microbe growth during incubation. Reactions were incubated in the dark at 37°C for 0, 1, 2, and 4 days before fluorescence reading with a Fluoroskan Ascent at excitation/emission of 480/530 nm.

Ependymal Cell Culture

EC cultures were adapted from a previous study (Paez-Gonzalez et al., 2011). All media contained L-glutamine and 1% penicillin/streptomycin. Minimum essential medium with HEPES was used for dissections. DMEM with 10% fetal bovine serum (FBS) was used to stimulate cell proliferation. DMEM with 2% FBS was used to induce EC differentiation. Papain solution, containing 1.2 μg/mL papain, 0.24 mg/mL L-cysteine, and 30 μg/mL DNaseI type IV dissolved in dissection medium was activated at 37°C for 30 min followed by sterile filtration. Tissue culture dishes were coated with 5 μg/mL poly-D-lysine at room temperature for at least 1 hr before being washed twice with sterile water. Lateral ventricular walls were dissected from P0–P1 mice in dissection medium and placed in a vial with 1 mL of dissection medium. Activated papain solution (200 μL) was added to each vial and incubated at 37°C for 20 min. The reaction was stopped by adding 2 mL of proliferation media. Tissue was mechanically dissociated with a fire polished Pasteur pipet in dissection medium. Dissociated cells were then switched into proliferation medium, and cells were plated at the density of 0.08 brains/cm^2 tissue culture surface. Cells reached confluence in 6–7 days and were switched to differentiation medium, in which cells differentiate into ECs for 6–12 days.

(H) Quantification of (E), (F), and (G) (left to right). Within H2B-CFP$^+$ cells, the percentage of SOX2$^+$ cells that are Ki67$^+$ is significantly increased by *Mmp12* shRNA (Ctrl shRNA, n = 3 mice; *Mmp12* shRNA, n = 3 mice; *p < 0.05, t test). The %Ki67$^+$ cells among MASH1$^+$ cells or the %MASH1$^+$ cells among SOX2$^+$ cells are not changed by *Mmp12* knockdown (WT, n = 4 mice; Mut, n = 4 mice; p > 0.05, t test). Error bars denote SEM. Dashed lines indicate ventricular surfaces. Scale bars, 10 μm.

Whole-Mount V-SVZ Immunohistochemistry

Whole-mount V-SVZ immunohistochemistry was adapted from a previous protocol (Mirzadeh et al., 2010a). In brief, mouse brains were dissected to expose the lateral ventricular walls. The tissue was submerged in 1% paraformaldehyde (PFA) in PBS and fixed at 4°C overnight. The tissue was subject to additional fixation with pre-chilled methanol-acetone (1:1) on ice for 10 min or heat-mediated antigen retrieval in sodium acetate buffer (pH 6), depending on the target antigen. Tissue was then washed with PBS and blocked in blocking solution (PBS containing 0.1% Triton X-100, 10% donkey serum) at room temperature for 1 hr, followed by primary antibody incubation overnight at 4°C, and secondary antibody incubation at room temperature for 2 hr. Antibodies were diluted in blocking solution. After washing, tissue was stained with DAPI for 10 min, and lateral walls were further dissected and mounted on glass slides with Slowfade Gold and coverslipped.

Streptavidin-Agarose Pull-Down Assay

The streptavidin-agarose pull-down assay was adapted from an existing protocol (Wu, 2006). In brief, 5′ biotinylated single-stranded oligos were dissolved to 100 mM in NaCl-Tris-EDTA buffer (pH 8.0). Complementary oligos were combined at 1:1 and incubated in a thermocycler at 95°C for 5 min, followed by −1.0°C per min for 70 min. HEK293T cells were transfected with XtremeGene HP transfection reagent. After 48 hr, cells were lysed on ice in 250 μL non-denaturing lysis buffer (25 mM Tris-HCl [pH 7.4], 100 mM NaCl, 1% Triton X-100, 1 mM PMSF) and cleared by centrifugation. The lysates were quantified with DC protein assay and adjusted to 8 mg/mL. Streptavidin-agarose beads were blocked in 4% BSA for 1 hr and 50 μL of the beads was used to pre-clear the lysate for 0.5 hr at room temperature. Pre-cleared cell lysate (250 μL) was then combined with 750 μL of PBS 1 mM with PMSF, 0.5 nM annealed oligo, and 50 μL of streptavidin-agarose beads, and incubated with gentle rotation at room temperature for 2 hr. The beads were then washed three times with PBS with 1 mM PMSF and boiled for 3 min with 50 μL 4× LDS sample buffer with 12% 2-mercaptoethanol. The eluate (25 μL) was used for western blotting.

Neonatal Ventricle Electroporation

Neonatal ventricle electroporation was adapted from a previous protocol (Feliciano et al., 2013). In brief, DNA constructs were purified with EndoFree Plasmid Maxi Kit and quantified with NanoDrop to ensure concentration >2 μg/μL, 260/230 > 2, and 1.8 < 260/280 < 2. P1 mice with milk spots were anesthetized using hypothermia. A 10-μL Hamilton syringe with 32-gauge needle was used for injection of 1 μL of DNA into the left lateral ventricle, at the middle point between the left eye and the center of lambda suture, and at the depth of 2–3 mm. The heads were then held with a tweezer electrode wet with PBS and subjected to electroporation at 5 square pulses, 100 V, 50 ms per pulse with 950-ms intervals, using an ECM 830 Generator. Mice recovered on a heating pad until resuming activity before being returned to their mothers.

SUPPLEMENTAL INFORMATION

Supplemental Information includes Supplemental Experimental Procedures, five figures, and one table and can be found with this article online at https://doi.org/10.1016/j.stemcr.2018.01.038.

AUTHOR CONTRIBUTIONS

H.C. and X.S. designed experiments, analyzed data, and wrote the manuscript. X.S., L.T., and Q.Y. conducted experiments.

ACKNOWLEDGMENTS

We thank Dr. David Anderson (Caltech) for the Mash1 antibody, Dr. Ken-Ichi Takemaru (Stony Brook University [SBU]) for FoxJ1 reporter mice, Dr. Kevin Czaplinski (SBU) for electroporation equipment, technical advice, and critical reading of the manuscript, Dr. Cindy Leiton (SBU) for *Mmp* primers, Ms. Alexa Lampasona (SBU) for assistance with 5′ RACE and critical reading of the manuscript, Dr. Steve Winder (University of Sheffield) for the βDAGΔNLS-EGFP construct, Dr. Maya Shelly (SBU) for electroporation equipment, and Dr. David Talmage (SBU) for critical reading of the manuscript.

Received: September 11, 2017
Revised: January 29, 2018
Accepted: January 30, 2018
Published: March 1, 2018

REFERENCES

Brizzi, M.F., Tarone, G., and Defilippi, P. (2012). Extracellular matrix, integrins, and growth factors as tailors of the stem cell niche. Curr. Opin. Cell Biol. *24*, 645–651.

Feliciano, D.M., Lafourcade, C.A., and Bordey, A. (2013). Neonatal subventricular zone electroporation. J. Vis. Exp. *72*, 50197. https://doi.org/10.3791/50197.

Gheusi, G., Cremer, H., McLean, H., Chazal, G., Vincent, J.D., and Lledo, P.M. (2000). Importance of newly generated neurons in the adult olfactory bulb for odor discrimination. Proc. Natl. Acad. Sci. USA *97*, 1823–1828.

Heissig, B., Hattori, K., Dias, S., Friedrich, M., Ferris, B., Hackett, N.R., Crystal, R.G., Besmer, P., Lyden, D., Moore, M.A., et al. (2002). Recruitment of stem and progenitor cells from the bone marrow niche requires MMP-9 mediated release of kit-ligand. Cell *109*, 625–637.

Houghton, A.M., Hartzell, W.O., Robbins, C.S., Gomis-Ruth, F.X., and Shapiro, S.D. (2009). Macrophage elastase kills bacteria within murine macrophages. Nature *460*, 637–641.

Jacquet, B.V., Salinas-Mondragon, R., Liang, H., Therit, B., Buie, J.D., Dykstra, M., Campbell, K., Ostrowski, L.E., Brody, S.L., and Ghashghaei, H.T. (2009). FoxJ1-dependent gene expression is required for differentiation of radial glia into ependymal cells and a subset of astrocytes in the postnatal brain. Development *136*, 4021–4031.

Jobin, P.G., Butler, G.S., and Overall, C.M. (2017). New intracellular activities of matrix metalloproteinases shine in the moonlight. Biochim. Biophys. Acta *1864* (11 Pt A), 2043–2055.

Kessenbrock, K., Dijkgraaf, G.J., Lawson, D.A., Littlepage, L.E., Shahi, P., Pieper, U., and Werb, Z. (2013). A role for matrix

metalloproteinases in regulating mammary stem cell function via the Wnt signaling pathway. Cell Stem Cell *13*, 300–313.

Larsen, P.H., DaSilva, A.G., Conant, K., and Yong, V.W. (2006). Myelin formation during development of the CNS is delayed in matrix metalloproteinase-9 and -12 null mice. J. Neurosci. *26*, 2207–2214.

Lee, C., Hu, J., Ralls, S., Kitamura, T., Loh, Y.P., Yang, Y., Mukouyama, Y.S., and Ahn, S. (2012). The molecular profiles of neural stem cell niche in the adult subventricular zone. PLoS One *7*, e50501.

Lehtinen, M.K., and Walsh, C.A. (2011). Neurogenesis at the brain-cerebrospinal fluid interface. Annu. Rev. Cell Dev. Biol. *27*, 653–679.

Li, L., and Xie, T. (2005). Stem cell niche: structure and function. Annu. Rev. Cell Dev. Biol. *21*, 605–631.

Lovett, D.H., Mahimkar, R., Raffai, R.L., Cape, L., Maklashina, E., Cecchini, G., and Karliner, J.S. (2012). A novel intracellular isoform of matrix metalloproteinase-2 induced by oxidative stress activates innate immunity. PLoS One *7*, e34177.

Marchant, D.J., Bellac, C.L., Moraes, T.J., Wadsworth, S.J., Dufour, A., Butler, G.S., Bilawchuk, L.M., Hendry, R.G., Robertson, A.G., Cheung, C.T., et al. (2014). A new transcriptional role for matrix metalloproteinase-12 in antiviral immunity. Nat. Med. *20*, 493–502.

McClenahan, F.K., Sharma, H., Shan, X., Eyermann, C., and Colognato, H. (2016). Dystroglycan suppresses notch to regulate stem cell niche structure and function in the developing postnatal subventricular zone. Dev. Cell *38*, 548–566.

Mercier, F. (2016). Fractones: extracellular matrix niche controlling stem cell fate and growth factor activity in the brain in health and disease. Cell. Mol. Life Sci. *73*, 4661–4674.

Mercier, F., Kitasako, J.T., and Hatton, G.I. (2002). Anatomy of the brain neurogenic zones revisited: fractones and the fibroblast/macrophage network. J. Comp. Neurol. *451*, 170–188.

Mirzadeh, Z., Merkle, F.T., Soriano-Navarro, M., Garcia-Verdugo, J.M., and Alvarez-Buylla, A. (2008). Neural stem cells confer unique pinwheel architecture to the ventricular surface in neurogenic regions of the adult brain. Cell Stem Cell *3*, 265–278.

Mirzadeh, Z., Doetsch, F., Sawamoto, K., Wichterle, H., and Alvarez-Buylla, A. (2010a). The subventricular zone en-face: whole-mount staining and ependymal flow. J. Vis. Exp. *39*, 1938. https://doi.org/10.3791/1938.

Mirzadeh, Z., Han, Y.G., Soriano-Navarro, M., Garcia-Verdugo, J.M., and Alvarez-Buylla, A. (2010b). Cilia organize ependymal planar polarity. J. Neurosci. *30*, 2600–2610.

Nagase, H., Visse, R., and Murphy, G. (2006). Structure and function of matrix metalloproteinases and TIMPs. Cardiovasc. Res. *69*, 562–573.

Nishida, C., Kusubata, K., Tashiro, Y., Gritli, I., Sato, A., Ohki-Koizumi, M., Morita, Y., Nagano, M., Sakamoto, T., Koshikawa, N., et al. (2012). MT1-MMP plays a critical role in hematopoiesis by regulating HIF-mediated chemokine/cytokine gene transcription within niche cells. Blood *119*, 5405–5416.

Obernier, K., Tong, C.K., and Alvarez-Buylla, A. (2014). Restricted nature of adult neural stem cells: re-evaluation of their potential for brain repair. Front. Neurosci. *8*, 162.

Ostrowski, L.E., Hutchins, J.R., Zakel, K., and O'Neal, W.K. (2003). Targeting expression of a transgene to the airway surface epithelium using a ciliated cell-specific promoter. Mol. Ther. *8*, 637–645.

Paez-Gonzalez, P., Abdi, K., Luciano, D., Liu, Y., Soriano-Navarro, M., Rawlins, E., Bennett, V., Garcia-Verdugo, J.M., and Kuo, C.T. (2011). Ank3-dependent SVZ niche assembly is required for the continued production of new neurons. Neuron *71*, 61–75.

Page-McCaw, A., Ewald, A.J., and Werb, Z. (2007). Matrix metalloproteinases and the regulation of tissue remodelling. Nat. Rev. Mol. Cell Biol. *8*, 221–233.

Porlan, E., Marti-Prado, B., Morante-Redolat, J.M., Consiglio, A., Delgado, A.C., Kypta, R., Lopez-Otin, C., Kirstein, M., and Farinas, I. (2014). MT5-MMP regulates adult neural stem cell functional quiescence through the cleavage of N-cadherin. Nat. Cell Biol. *16*, 629–638.

Relucio, J., Menezes, M.J., Miyagoe-Suzuki, Y., Takeda, S., and Colognato, H. (2012). Laminin regulates postnatal oligodendrocyte production by promoting oligodendrocyte progenitor survival in the subventricular zone. Glia *60*, 1451–1467.

Sakamoto, M., Imayoshi, I., Ohtsuka, T., Yamaguchi, M., Mori, K., and Kageyama, R. (2011). Continuous neurogenesis in the adult forebrain is required for innate olfactory responses. Proc. Natl. Acad. Sci. USA *108*, 8479–8484.

Sawamoto, K., Wichterle, H., Gonzalez-Perez, O., Cholfin, J.A., Yamada, M., Spassky, N., Murcia, N.S., Garcia-Verdugo, J.M., Marin, O., Rubenstein, J.L., et al. (2006). New neurons follow the flow of cerebrospinal fluid in the adult brain. Science *311*, 629–632.

Shapiro, S.D., Griffin, G.L., Gilbert, D.J., Jenkins, N.A., Copeland, N.G., Welgus, H.G., Senior, R.M., and Ley, T.J. (1992). Molecular cloning, chromosomal localization, and bacterial expression of a murine macrophage metalloelastase. J. Biol. Chem. *267*, 4664–4671.

Shapiro, S.D., Kobayashi, D.K., and Ley, T.J. (1993). Cloning and characterization of a unique elastolytic metalloproteinase produced by human alveolar macrophages. J. Biol. Chem. *268*, 23824–23829.

Shen, Q., Wang, Y., Kokovay, E., Lin, G., Chuang, S.M., Goderie, S.K., Roysam, B., and Temple, S. (2008). Adult SVZ stem cells lie in a vascular niche: a quantitative analysis of niche cell-cell interactions. Cell Stem Cell *3*, 289–300.

Shigemoto-Mogami, Y., Hoshikawa, K., Goldman, J.E., Sekino, Y., and Sato, K. (2014). Microglia enhance neurogenesis and oligodendrogenesis in the early postnatal subventricular zone. J. Neurosci. *34*, 2231–2243.

Shimizu-Hirota, R., Xiong, W., Baxter, B.T., Kunkel, S.L., Maillard, I., Chen, X.W., Sabeh, F., Liu, R., Li, X.Y., and Weiss, S.J. (2012). MT1-MMP regulates the PI3Kdelta.Mi-2/NuRD-dependent control of macrophage immune function. Genes Dev. *26*, 395–413.

Shipley, J.M., Wesselschmidt, R.L., Kobayashi, D.K., Ley, T.J., and Shapiro, S.D. (1996). Metalloelastase is required for macrophage-mediated proteolysis and matrix invasion in mice. Proc. Natl. Acad. Sci. USA *93*, 3942–3946.

Shook, B.A., Manz, D.H., Peters, J.J., Kang, S., and Conover, J.C. (2012). Spatiotemporal changes to the subventricular zone stem cell pool through aging. J. Neurosci. *32*, 6947–6956.

Warner, R.L., Lukacs, N.W., Shapiro, S.D., Bhagarvathula, N., Nerusu, K.C., Varani, J., and Johnson, K.J. (2004). Role of metalloelastase in a model of allergic lung responses induced by cockroach allergen. Am. J. Pathol. *165*, 1921–1930.

Wu, K.K. (2006). Analysis of protein-DNA binding by streptavidin-agarose pulldown. Methods Mol. Biol. *338*, 281–290.

Zhang, Z., Amorosa, L.F., Coyle, S.M., Macor, M.A., Lubitz, S.E., Carson, J.L., Birnbaum, M.J., Lee, L.Y., and Haimovich, B. (2015). Proteolytic cleavage of AMPKalpha and intracellular MMP9 expression are both required for TLR4-mediated mTORC1 activation and HIF-1alpha expression in leukocytes. J. Immunol. *195*, 2452–2460.

Stem Cell Reports, Volume *10*

Supplemental Information

Distinct Requirements for Extracellular and Intracellular MMP12 in the Development of the Adult V-SVZ Neural Stem Cell Niche

Xiwei Shan, Lyl Tomlinson, Qian Yang, and Holly Colognato

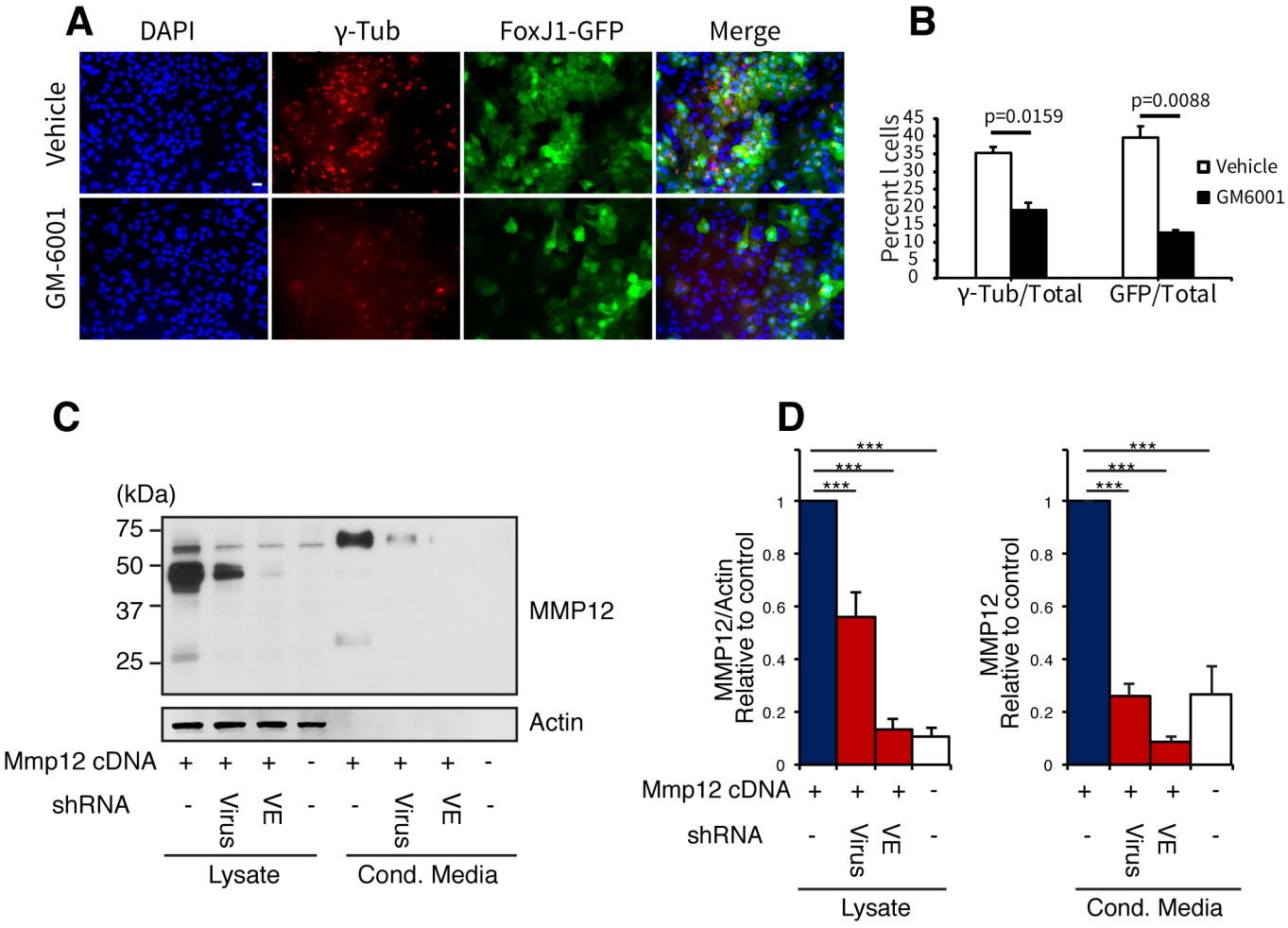
A
DAPI
γ-Tub
FoxJ1-GFP
Merge
Vehicle
GM-6001
B
Percent l cells
p=0.0159
p=0.0088
Vehicle
GM6001
γ-Tub/Total
GFP/Total
C
(kDa)
75
50
37
25
MMP12
Actin
Mmp12 cDNA
shRNA
Virus
VE
Lysate
Cond. Media
D
MMP12/Actin
Relative to control
MMP12
Relative to control
***

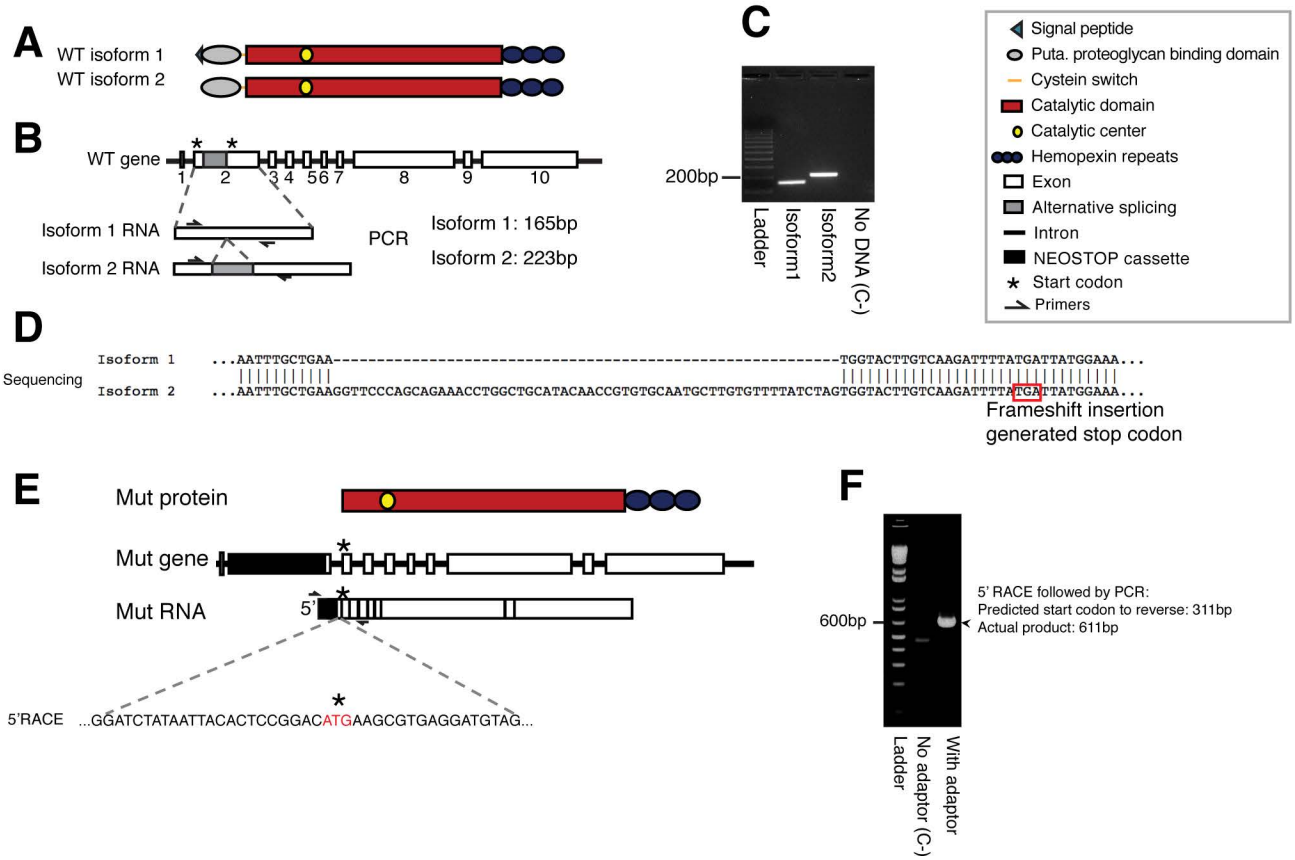
A
WT isoform 1
WT isoform 2
B
WT gene
1 2 3 4 5 6 7 8 9 10
Isoform 1 RNA
Isoform 2 RNA
PCR
Isoform 1: 165bp
Isoform 2: 223bp
C
200bp
Ladder
Isoform1
Isoform2
No DNA (C-)
Signal peptide
Puta. proteoglycan binding domain
Cystein switch
Catalytic domain
Catalytic center
Hemopexin repeats
Exon
Alternative splicing
Intron
NEOSTOP cassette
Start codon
Primers
D
Sequencing
Isoform 1 ...AATTTGCTGAA----------TGGTACTTGTCAAGATTTTATGATTATGGAAA...
Isoform 2 ...AATTTGCTGAAGGTTCCCAGCAGAAACCTGGCTGCATACAACCGTGTGCAATGCTTGTGTTTTATCTAGTGGTACTTGTCAAGATTTTATGATTATGGAAA...
Frameshift insertion
generated stop codon
E
Mut protein
Mut gene
Mut RNA
5'
5'RACE ...GGATCTATAATTACACTCCGGACATGAAGCGTGAGGATGTAG...
F
600bp
5' RACE followed by PCR:
Predicted start codon to reverse: 311bp
Actual product: 611bp
Ladder
No adaptor (C-)
With adaptor

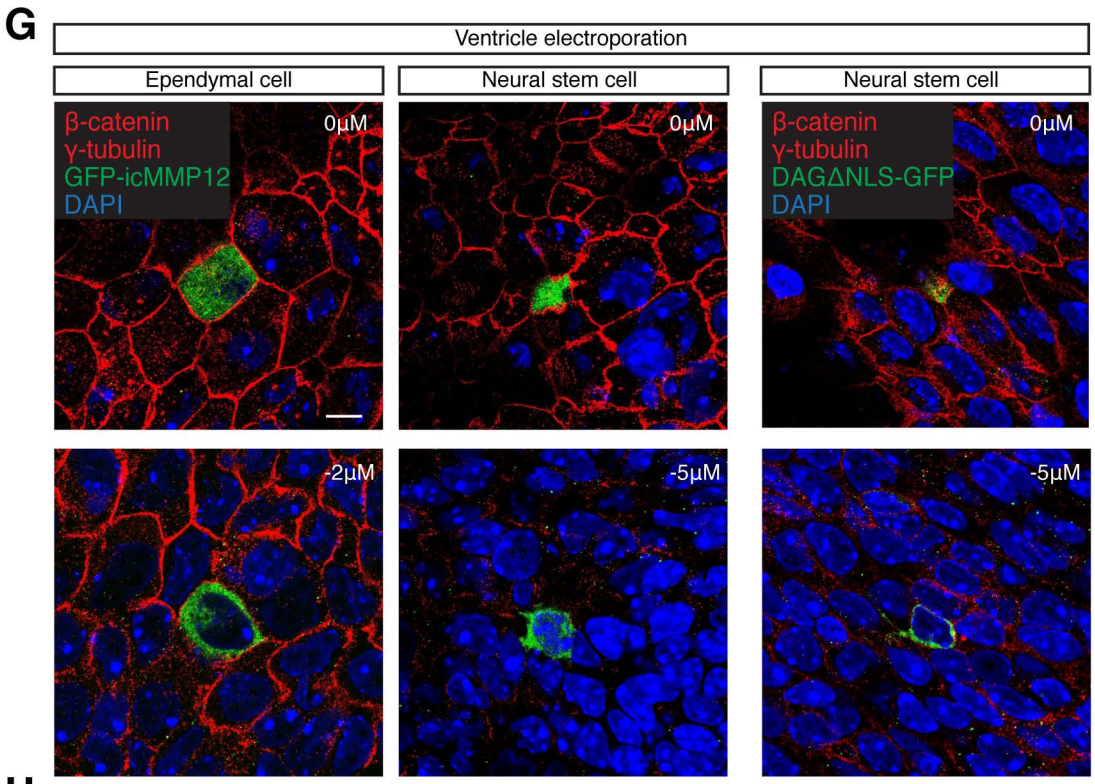
G
Ventricle electroporation
Ependymal cell
Neural stem cell
Neural stem cell
β-catenin
γ-tubulin
GFP-icMMP12
DAPI
0μM
β-catenin
γ-tubulin
DAGΔNLS-GFP
DAPI
0μM
-2μM
-5μM
-5μM

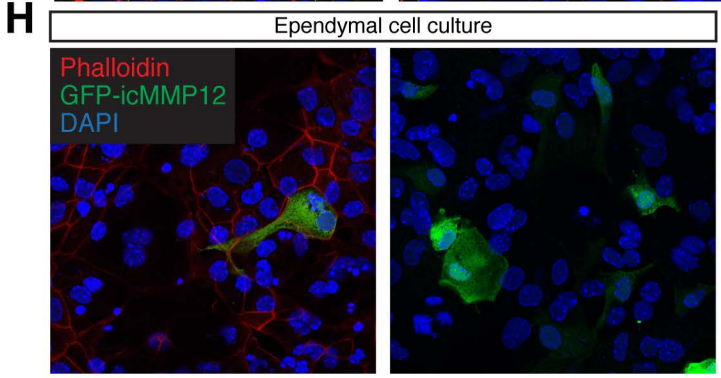
H
Ependymal cell culture
Phalloidin
GFP-icMMP12
DAPI

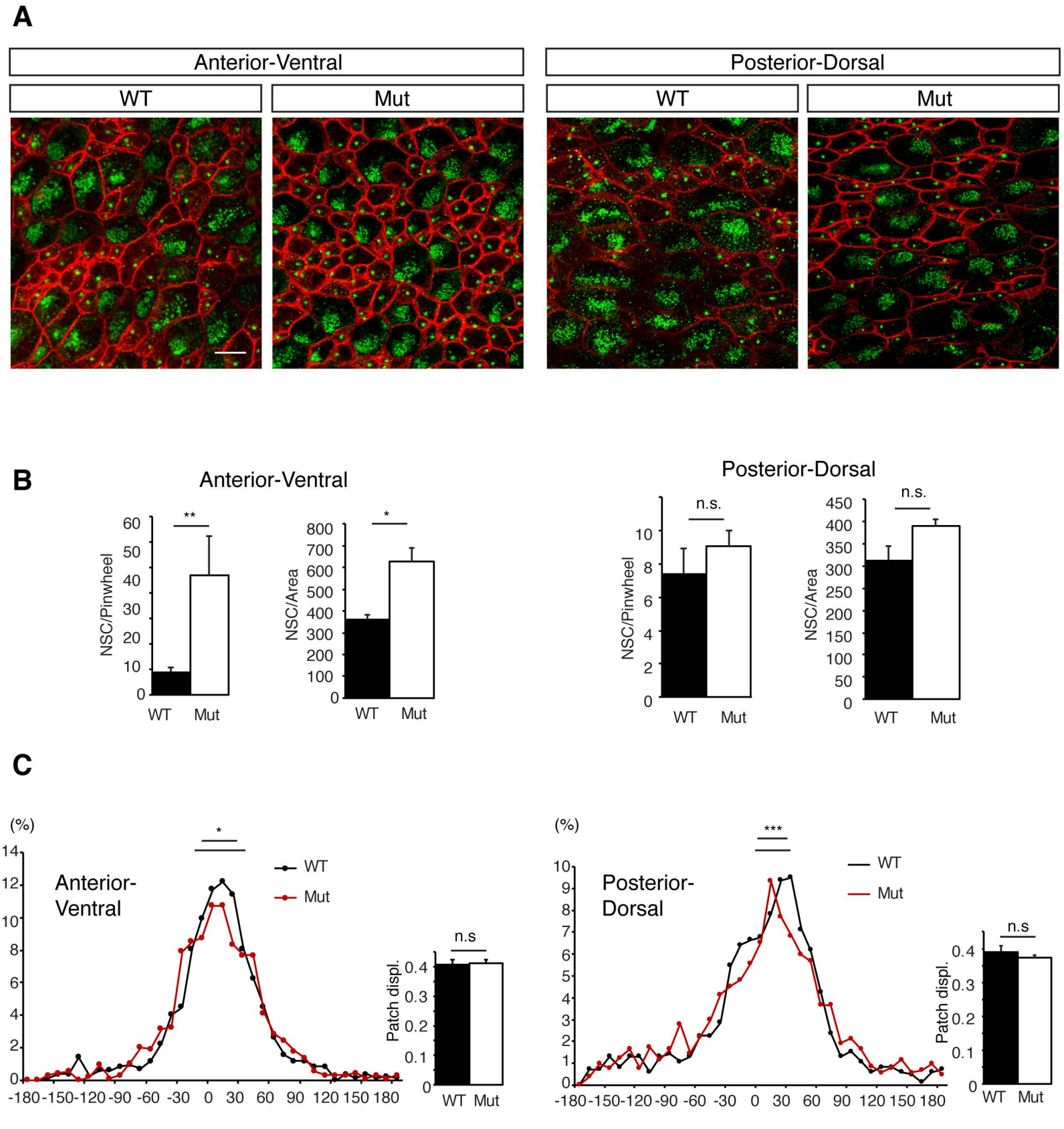
A
Anterior-Ventral
Posterior-Dorsal
WT
Mut
WT
Mut
B
Anterior-Ventral
Posterior-Dorsal
NSC/Pinwheel
NSC/Area
**
*
n.s.
n.s.
WT
Mut
C
(%)
*
***
Anterior-
Ventral
Posterior-
Dorsal
WT
Mut
Patch displ.
n.s
-180 -150 -120 -90 -60 -30 0 30 60 90 120 150 180

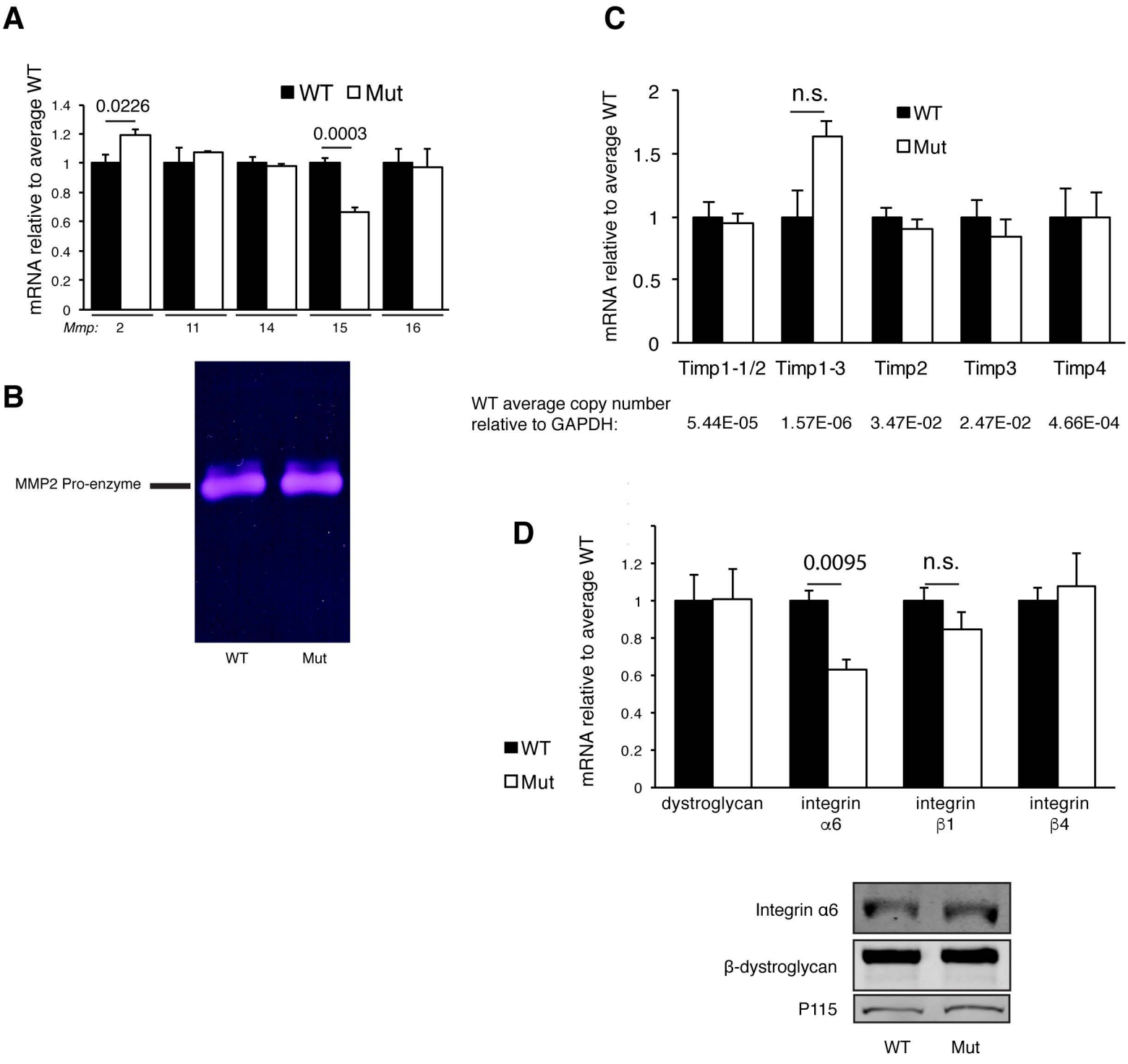
A
mRNA relative to average WT
WT
Mut
0.0226
0.0003
Mmp:
2
11
14
15
16
B
MMP2 Pro-enzyme
WT
Mut
C
mRNA relative to average WT
n.s.
WT
Mut
Timp1-1/2
Timp1-3
Timp2
Timp3
Timp4
WT average copy number relative to GAPDH:
5.44E-05
1.57E-06
3.47E-02
2.47E-02
4.66E-04
D
mRNA relative to average WT
0.0095
n.s.
WT
Mut
dystroglycan
integrin α6
integrin β1
integrin β4
Integrin α6
β-dystroglycan
P115
WT
Mut

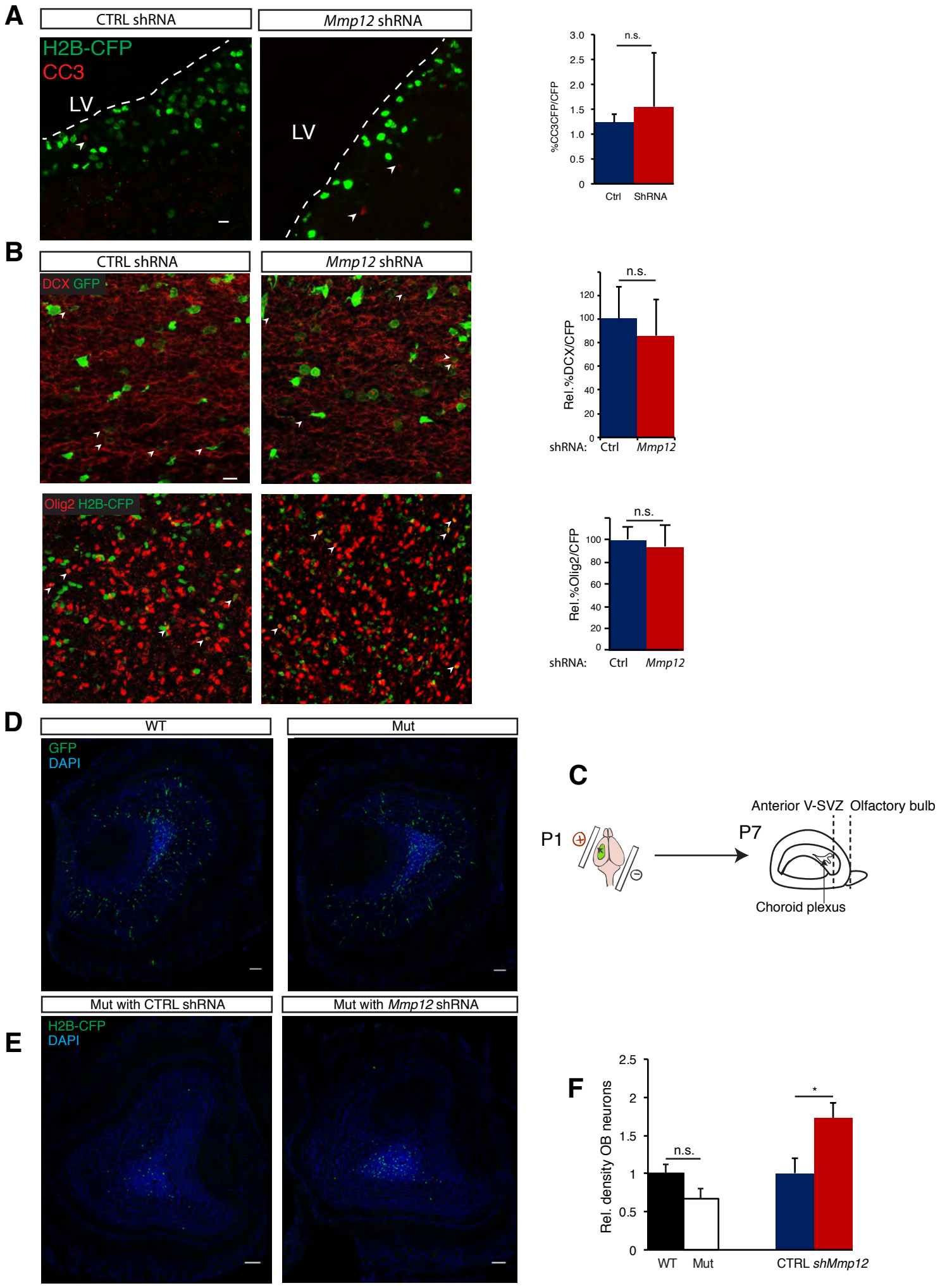
A
CTRL shRNA
Mmp12 shRNA
H2B-CFP
CC3
LV
LV
n.s.
%CC3CFP/CFP
3.0
2.5
2.0
1.5
1.0
0.5
0
Ctrl
ShRNA
B
CTRL shRNA
Mmp12 shRNA
DCX GFP
n.s.
Rel.%DCX/CFP
120
100
80
60
40
20
0
shRNA:
Ctrl
Mmp12
Olig2 H2B-CFP
n.s.
Rel.%Olig2/CFP
100
80
60
40
20
0
shRNA:
Ctrl
Mmp12
D
WT
Mut
GFP
DAPI
C
Anterior V-SVZ
Olfactory bulb
P1
P7
Choroid plexus
E
Mut with CTRL shRNA
Mut with Mmp12 shRNA
H2B-CFP
DAPI
F
Rel. density OB neurons
2.5
2
1.5
1
0.5
0
n.s.
*
WT
Mut
CTRL shMmp12

Supplemental Figure Legends

Figure S1. General inhibition of MMP activity blocks FoxJ1 transcription and ciliogenesis in ependymal cells. Related to Figs. 1 and 5 (shRNA confirmation). **A-B.** Ependymal cell cultures generated from FoxJ1-promoter driven GFP reporter mice were treated with vehicle (DMSO) or 25μM GM-6001 during differentiation, and analyzed via immunohistochemistry (IHC) at differentiation day 6. A. Representative images. B. Quantification. The percentages of multiciliated cells and GFP+ cells are both significantly reduced in GM-6001-treated group. n=3 for each group; scale bar = 20μm **C-D.** Lentivirus shRNA ("virus") plasmid and ventricle electroporation (VE) shRNA plasmids were transfected into 293T cells expressing full-length MMP12 cDNA. Corresponding plasmids without insert (designated as "-" in each condition) were used as transfection controls. Western blots indicate a substantial reduction of MMP12 protein in both cell lysates and conditioned media. **C.** Representative blot. **D.** Quantification (n = 5 for cell lysates, n = 3 for conditioned media. Conditioned media loading volume was adjusted based on protein quantification of cell lysate from the corresponding dish, and quantification was normalized to the actin of this corresponding lysate. *** $p<0.001$ by one-way ANOVA followed by multicomparison with Turkey-Kramer correction).

Figure S2. Characterization of icmmp12 transcripts in WT and Mut and icMMP12 subcellular localization in the V-SVZ. Related to Fig. 2. **A-F.** Both WT and *mmp12* mutant ependymal cells contain icMMP12-encoding transcripts. **A**. WT isoform 1 contains signal peptide sequence and therefore can be secreted. Isoform 2 has an inserted sequence in exon 2 resulting in a frameshift and alternative translational initiation. **B.** PCR using primers targeting common sections of isoform 1 and 2 yields products of different sizes. **C.** Agarose gel of the PCR products that were cloned into pcDNA3.1(+). Band sizes agree with the predicted produce sizes of isoform 1, and 2. **D.** Sequencing results of the PCR products that were cloned into pcDNA3.1(+), results are aligned and as predicted, corresponding with isoform 1 and 2 respectively. **E.** 5' RACE identified an intracellular *mmp12* mRNA, with the indicated start codon (asterisks) as the only in-frame ATG. The mRNA contains a small portion of the neo-STOP cassette inserted into mutant genome (black box). **F.** Agarose gel of the 5' RACE products without (middle lane) or with (right lane) the 5' adaptor. **G-H.** icMMP12 in V-SVZ cells translocate into nucleus. **G.** WT neonatal mice were electroporated with GFP-icMMP12 or DAGΔNLS-GFP (negative control) and assessed by wholemount immunohistochemistry at P7. Confocal images indicate modest nuclear localization of icMMP12 in ependymal cells and more extensive nuclear localization in neural stem cells. In contrast DAGΔNLS-GFP was not observed in the nucleus. **H.** Ependymal cell cultures were transfected with GFP-icMMP12 using XtremeGene-HP. Nuclear staining was observed in GFP+ cells at differentiation day 6.

Figure S3. Assessment of neural stem cell niche pinwheel organization and planar cell polarity in anterior-ventral (AV) and posterior-dorsal (PD) V-SVZ. Related to Figs. 3 (C, D) and 4. **A-C.** Left panel: AV V-SVZ. Right panel: PD V-SVZ. **A.** Representative images of AV and PD V-SVZ in WT and *mmp12* mutant (Mut) mice at P7. **B.** There are more NSCs per pinwheel and NSCs per area in the AV, but not PD, V-SVZ of *mmp12* mutant mice. (*$p<0.05$, **$p<0.01$ by t-test) **C.** Cilia patch angle distribution in both the AV and PD V-SVZ are disturbed in *mmp12* mutant mice (*$p<0.05$, ***$p<0.001$ by Watson's U2 test). Patch displacement is unchanged in either the AV or PD V-SVZ (t-test). AV-WT n = 842, AV-Mut n = 948, PD-WT n = 851, PD-Mut n= 1038, WT: 4 animals, Mut: 4 animals. Scale bar = 10μm.

Figure S4. Analysis of MMP and TIMP expression in *mmp12* mutant ependymal cells. Related to Fig.3 (E-G). **A.** RT-qPCR results of *mmp2, 11, 14, 15*, and *16* in ependymal cell (EC) cultures from WT and *mmp12* mutant (Mut) mice at differentiation day 6. *Mmp12* transcription is upregulated while *mmp15* (*mt2-mmp*) is downregulated (WT, n=6; Mut, n=8) **B.** On-gel gelatin zymography of conditioned media from WT and Mut EC cultures. No noticeable band is present for activated MMP2, and the pro band appears similar in both genotypes. **C.** RT-qPCR indicates mRNA level of timps are not changed in Mut. Note that the Timp1 transcription variant 3 (Timp1-3) has much lower copy number compare to variant 1 and 2 (Timp1-1/2). WT, n = 7; Mut, n = 8. **D.** RT-

qPCR indicates mRNA level of dystroglycan, integrin β1, and integrin β4 genes are not changed in Mut ECs. While mRNA level of integrin α6 is lower in Mut ECs ($p=0.0095$, $n=3$), western blotting did not indicate any change in integrin α6 or β-dystroglycan protein levels.

Figure S5. Assessment of additional niche features upon loss of extracellular and intracellular MMP12. Related to Figs. 5 and 6. **A.** V-SVZ apoptosis following loss of icMMP12. *mmp12* mutant mice were electroporated with control shRNA or *mmp12* shRNA coexpressing H2B-CFP at p1 and coronal brain sections were assessed at p7. Apoptotic cells were labeled with cleaved caspase 3 (CC3) antibody. CFP and CC3 double positive cells were quite rare (less than 2%) and never observed in the ependymal cell layer. No significant increase was observed in the *mmp12* shRNA group (by t-test, n = 3 for each group). Scale bar = 10μm. **B.** Neurogenesis and gliogenesis following loss of icMMP12. *mmp12* mutant mice were electroporated with control shRNA or *mmp12* shRNA coexpressing GFP (for DCX co-IHC) or H2B-CFP (for Olig2 co-IHC) at p1 and wholemounts were assessed at p7. Left: Representative images of DCX+GFP (upper) and Olig2+H2B-CFP (lower) wholemount IHC. Arrowheads: double positive cells. Right: Quantification of %DCX/GFP and %Olig2/CFP cells in the entire wholemounts. No significant differences were found (by t-test). DCX+GFP: *ctrl* shRNA n = 3, *mmp12* shRNA n = 3, Olig2+H2B-CFP: *ctrl* shRNA n = 5, *mmp12* shRNA n = 4. Scale bar = 20μm. **C-F**. Rostral migration to the olfactory bulb (OB). **C.** Mice were electroporated at p1 and coronal sections of anterior V-SVZ and OB were analyzed at p7. Representative images of OBs from WT and *mmp12* mutant (Mut) mice electroporated with GFP plasmid. **E.** Representative images of OBs from Mut mice electroporated with control (ctrl) shRNA or *mmp12* shRNA co-expressing H2B-CFP. F. Quantification of relative GFP or CFP+ cells in the OB. Electroporation efficiency is normalized by number of GFP+ or CFP+ cells in the anterior SVZ. Normalized number of CFP+ cells in the OB is significantly increased in *mmp12* shRNA group compared to control. WT n = 4; Mut n = 4; *ctrl* shRNA n = 5; *mmp12* shRNA n = 4. *$p<0.05$ by t-test. Scale bar = 100μm.

Table S1. MMP transcript levels in differentiating ependymal cell cultures (related to Fig.1B). Results are generated from pooled samples of 3 indipendent experiments for each time point.

Max<	MMP	Day 1	Day 6	Day 12
10^-2	14	5.56E-03	4.42E-03	3.88E-03
	12	1.12E-04	1.27E-03	4.65E-03
	15	1.77E-03	1.74E-03	1.62E-03
	16	1.68E-03	1.21E-03	1.22E-03
10^-3	2	7.23E-04	2.87E-04	1.79E-04
	11	4.96E-04	5.50E-04	6.07E-04
10^-4	24	1.32E-04	3.82E-05	3.45E-05
	17	1.29E-04	5.17E-05	3.06E-05
	23	6.22E-05	6.46E-05	5.50E-05
	21	5.50E-05	3.71E-05	4.83E-05
	28A	3.95E-05	2.24E-05	2.91E-05
	28B	3.57E-05	3.43E-05	3.66E-05
	19B	1.55E-05	2.77E-05	3.29E-05
	9	2.34E-06	4.93E-06	2.17E-05
	13	1.38E-06	3.80E-06	1.04E-05
10^-5	19A	4.23E-06	5.29E-06	8.12E-06
	7	4.15E-06	2.27E-06	2.88E-06
	27	1.50E-07	1.28E-06	3.07E-06
	3	3.28E-07	1.41E-06	2.85E-06
	25	6.25E-07	9.02E-07	1.07E-06
10^-6	10	6.53E-07	7.21E-07	8.20E-07
	8	8.15E-08	2.72E-07	2.55E-07
	20	1.64E-07	1.35E-07	9.85E-08
	1	3.35E-08	1.21E-07	1.06E-07

Supplemental Experimental Procedures

Planar cell polarity analysis

```
%% Run each section separately.
%% UI Import: Arrange results from each image into a single column. Import as the form of numeric matrix.For wilde type name import as WT, knockout name KO.

%% WT
[NumRow, NumClmn] = size(WT);
FixedWT = WT;
% M is an array of means of each image.
M = nanmean(WT);

% Loop for going through each image(column).
for c = 1:NumClmn;

 %To prevent shift of mean after fixing number,
 %Possibly need several fixes.
 while abs(M(c)) >= 0.1;
        FixedWT(:,c) = FixedWT(:,c) - M(c);
  %Going through each number in an image.
    for r = 1:NumRow
       %Shift overflowing numbers
        if FixedWT(r,c) >= 180
        FixedWT(r,c) = FixedWT(r,c) - 360;
          elseif FixedWT(r,c) < -180
            FixedWT(r,c) = FixedWT(r,c) + 360;
            %else includes NaN.
                else FixedWT(r,c) = FixedWT(r,c);
        end

    end

      M(c) = nanmean(FixedWT(:,c));
 end


end
% Combine array into a single vector and get rid of NaN.
FixedWTstrng = FixedWT(:);
FixedWTstrng(isnan(FixedWTstrng(:,1)),:)=[];

%% KO
[NumRow, NumClmn] = size(KO);
FixedKO = KO;
% M is an array of means of each image.
M = nanmean(KO);

% Loop for going through each image(column).
for c = 1:NumClmn;

 %To prevent shift of mean after fixing number,
 %Possibly need several fixes.
 while abs(M(c)) >= 0.1;
```

```
        FixedKO(:,c) = FixedKO(:,c) - M(c);
  %Going through each number in an image.
    for r = 1:NumRow
       %Shift overflowing numbers
        if FixedKO(r,c) >= 180
        FixedKO(r,c) = FixedKO(r,c) - 360;
          elseif FixedKO(r,c) < -180
            FixedKO(r,c) = FixedKO(r,c) + 360;
            %else includes NaN.
                else FixedKO(r,c) = FixedKO(r,c);
        end

    end

      M(c) = nanmean(FixedKO(:,c));
 end


end
% Combine array into a single vector and get rid of NaN.
FixedKOstrng = FixedKO(:);
FixedKOstrng(isnan(FixedKOstrng(:,1)),:)=[];

%% plot histogram of W|T/K|O.

Hst = zeros(37,2);
[NumWT,~] = size(FixedWTstrng);
[NumKO,~] = size(FixedKOstrng);
N = [NumWT, NumKO];


 for i = (1:36);
       Find = and(FixedWTstrng >= -180 + (i-1)*10,...
                FixedWTstrng < -180 + i*10);
       Perc = sum(Find)/N(1,1);
       Hst(i,1) = Perc;
 end
 for i = (1:36);
       Find = and(FixedKOstrng >= -180 + (i-1)*10,...
                FixedKOstrng < -180 + i*10);
       Perc = sum(Find)/N(1,2);
       Hst(i,2) = Perc;
 end

Y1 = 100*Hst(:,1);
Y2 = 100*Hst(:,2);
X = -180: 10: 180;
plt = plot(X, Y1, 'k',X, Y2, 'r');
 % line styles.
 plt(1).LineWidth= 2;
 plt(1).Marker='o';
 plt(1).MarkerSize= 4;
 plt(1).MarkerEdgeColor= 'k';
 plt(1).MarkerFaceColor= 'k';
 plt(2).LineWidth= 2;
 plt(2).Marker='o';
```

```
 plt(2).MarkerSize= 4;
 plt(2).MarkerEdgeColor= 'r';
 plt(2).MarkerFaceColor= 'r';


 % Axis range and style.
axis([-180 180 0 10])
set(gca, 'XTick', [-180, -150, -120, -90, -60, -30, 0,...
    30, 60, 90, 120, 150, 180])
set(gca,'box','off')

 % Axis label.
x = xlabel('(o)');
set(x, 'position', get(x, 'position')+[190,0,0]);
y = ylabel('(%)', 'rot', 0);
set(y, 'position', get(y, 'position')+[-10,5,0]);

 % Legend
Lg = legend('WT', 'KO');
set(Lg,'box','off')

%% U2 test
[p,~,~] = watsons_U2_perm_test(FixedWTstrng, FixedKOstrng, 1000);
```

Primers and DNA oligonucleotides

Name	Forward	Reverse	Product size
MMP1a	GCAGGAAGGAGGCCACTGGTGAT	TCCACATTTTGCCGGTCTCCGTTG	135
MMP1b	GCTTCCTGCCAGAACCTTTGATCG	TGCTGCCTTTGAAAAAGCGGAGT	120
MMP2	TCTGCCCCCATGAAGCCTTGT	GTGCCCTGGAAGCGGAACGG	82
MMP3	CCTGCTGTGGCTGTGTGTGGTT	TCCCTGTCATCTCCAACCCGAGGA	215
MMP7	CAGGCCTAGGCGGAGATGCTCA	GCAATGGAGGACCCAGTGAGTGC	297
MMP8	TGGCCCTTCCTACCCAACGGT	AGAGCCCAGTACTGTCTGCCTTT	92
MMP9	GCTGGGCAAAGGCGTCGTGAT	CGTCTGTGGTGCAGGCCGAA	110
MMP10	GTGACACAAGGCCACCCAAGCA	CACCACACCTGGGCTTGTGCAT	211
MMP11	GCCTGTCTCCTCCGCGCGAT	ACGGTGACTCTCCGGTGGCCT	120
MMP12	TGCATTTGGAGCTCACGGAGAC	TGCTGCAGCCCCAAGGAATGG	195
MMP13	AAGACAGATTCTTCTGGCGCCTG	AGTGAACCGCAGCGCTCAGTC	252
MMP14	AAAACCCCGCCTATGGGCCC	GCCAGAACCATCGCTCCTTGA	100
MMP15	GGGTACATGTGAAAGCCAACCT	GGTAATTGTTCCATGCCTTTCC	75
MMP16	CCCGGAGAGCAATTCGCCGT	TCGCCTCCAATTCCGGGTCCA	214
MMP17	CCGTGGGTGACCCGCTACGC	CCCGCACACCGTACAACTGCC	78
MMP19a	GGCTGGCATTCTTACTTCCCATGAC	TCTCCAGTGGCCCAGAAGCAGG	299
MMP19b	AGCAAAGACCTGGAGGATTACCTGT	GCTGCTTCATACGGGCCCTTGT	175
MMP20	ACAGATGGCCCTGCATGCGT	TCCGGGGTCCGTATAATGCTTGG	395
MMP21	CAA AGG CAA CTC GTA CTG GA	AAC CAC TTC TCG GAA ACA GG	108
MMP23	TGATTTCTGTTATGAATTCCCATTTC	TCTCTCACCAACCTTGTTTTCGT	81
MMP24	GTG ATG AGG CCA GTA TGG TG	AAC AGG ATG CCC GCT AGT AT	95
MMP25	AGAAGACGTGGATGCTGTGTTCT	TTTGACCTCGGATCAGGTATGTC	65
MMP27	TTCTGTCTTGCCCGGTTACC	CAGACGGCTGCATCAATTTTC	81
MMP28a	TGGCAATGTTTCAGAGCCTCGTCCA	GTGCGAACCCCCACACGGAC	161
MMP28b	CCATCACTGTAGAGCCTCGTCCAC	GTGCGAACCCCCACACGGAC	159
MMP12 Exon1	GAACTTGCAGTCGGAGGGAA	TGTCATTCATGGGAGCAGCC	127
MMP12 Exon4/5	TTGCATTTGGAGCTCACGGA	ATGTCATCAGCAGAGAGGCG	277
MMP12 Exon7/8	TCCATATGGCCAAGCATCCC	TTGGCGAAGTGGGTCAAAGA	204
GAPDH	GCACAGTCAAGGCCGAGAAT	GCCTTCTCCATGGTGGTGAA	151
5'RACE Outer	GCTGATGGCGATGAATGAACACTG	ATGTCATCAGCAGAGAGGCG	n.a.
5'RACE Inner	CGCGGATCCGAACACTGCGTTTGCTGGCTTTGATG	TGCTGCAGCCCCAAGGAATGG	611
Isoform ID Outer	GCTGCTCCCATGAATGACAGT	GATGCTGTACATCGGGCACT	229/287/147
Isoform ID Inner	GCTGCTCCCATGAATGACAGT	TTGCCCAGTTGCTTCTAGCC	165/223/83

Biotinylated oligos for Streptavidin-agarose pull-down assays:
Biotin-5'-ACAAACATTAACACCTTGCTTTACTTGGGAAACAAAAAAAATCATGGTCC
Biotin-5'-GGACCATGATTTTTTTTGTTTCCCAAGTAAAGCAAGGTGTTAATGTTTGT

shRNA targeting sequences:
Mmp12 shRNA#1 target (ventricle electroporation): CATTTCGCCTCTCTGCTGATGACATACGT
Mmp12 shRNA#2 target (lentivirus transduction): TACTACATCTTCCAAGGAGCCTATCAATT
Mmp14 shRNA target (lentivirus transduction): GACACAGAGAACTTCGTGTTGCCTGATGA
Scrambled sequence: GTCCGTCTTCGCGCCATATCTCTAGTATA

Antibodies

Antigen	Company	Catalog#	Species	Applications	Dilution
MMP12	R&D Systems	AF3467	Goat	WB	1:1000
MMP12	Abcam	ab66157	Rabbit	IHC	1:100
Sox2	Abcam	ab97959	Rabbit	IHC	1:200
Sox2	R&D Systems	245610	Mouse	IHC	1:100
Mash1	Gift from Dr. David Anderson	N.A.	Mouse	IHC	1:2
Ki67	eBioscience	14-5698	Rat	IHC	1:500
FoxJ1	eBioscience	14-9965-82	Mouse	IHC	1:100
GFP	Aves Labs	GFP-1020	Chicken	IHC	1:600
GFP	Molecular Probs	A11122	Rabbit	WB	1:1000
β-catenin	BD Biosciences	610153	Mouse	IHC	1:300
β-catenin (non-phospho)	CST	19807	Rabbit	IHC	1:1000
γ-tubulin	Sigma	T5192	Rabbit	IHC	1:1000
Acetylated tubulin	Sigma	T6793	Mouse	IHC	1:1000
CD24	BD Biosciences	557436	Rat	IHC	1:100
Pan-laminin	Sigma	L9393	Rabbit	WB, IHC	1:1000
DCX	Abcam	AB18723	Rabbit	IHC	1:1000
Olig2	IBL	18953	Rabbit	IHC	1:100
CC3	Cell Signaling	9661	Rabbit	IHC	1:250
p115	BD Biosciences	612261	Mouse	WB	1:5000
β-actin	Sigma	A5441	Mouse	WB	1:5000
Phalloidin-FITC	Thermo Fisher	F432	N.A.	IHC	1:100
DAPI	Sigma	D9542-1MG	N.A.	IHC	10ug/ml

DNA constructs and molecular cloning
The following plasmids were used in this study: pH2B-GFP-SUPER (Colognato et al., 2004), pEF1-V5-HisA (invitrogen), pCDNA3.1(+) (invitrogen), pEGFP-C1(BD Biosciences, #6084-1), pCIG2 (Hand et al., 2005), PLB (Addgene, #11619)(Kissler et al., 2006). Full length *mmp12* and *ic-mmp12* cDNA was cloned into pEF1-V5-HisA at BamH1 and XhoI sites. Full length *mmp12* and *ic-mmp12* catalytic domain containing an artificial Kozak sequence and tethered with C-terminal 7xHis was cloned into pCDNA3.1(+) at BamH1 and XhoI. *ic-mmp12* cDNA was cloned into pCIG2 at XhoI and XmaI. *ic-mmp12* cDNA was cloned into pEGFP-C1 at XhoI and SpeI. shRNA was cloned into pH2B-GFP-SUPER by BglII and HindIII, into pLB by HpaI and XhoI. All cloning reagents were from NEB.

Reverse Transcription quantitative Polymerase Chain Reaction (RT-qPCR)
Cells were lysed in 500µl of Qiazol (Qiagen) and stored in -80°C until RNA extraction. Total mRNA was extracted using an RNeasy Mini Kit (Qiagen) with on-column DNase treatment (Qiagen). Eluted RNA was quantified with NanoDrop 1000. A260/280>2.0, A260:230>2.0. 500-1000ng of total RNA per 20µl reaction was used for reverse transcription with Protoscript M-MuLV First Strand cDNA Synthesis Kit (NEB). qPCR was performed with Fast SYBR Green Master Mix (Applied Biosystems) with a StepOnePlus Real-Time PCR System. Between 1 and 50ng of cDNA was loaded per µL reaction, depending on target abundance.

5' Rapid Amplification of cDNA Ends (RACE)
Total RNA was extracted from *mmp12* mutant ependymal cell cultures at differentiation day 12, and 5' RACE was carried out using FirstChoice RLM-RACE Kit. PCR was carried out with Phusion High-Fidelity PCR Master Mix and cleaned with QIAquick PCR Purification Kit (Qiagen) before sequencing.

Protein purification
270 µg pCDNA3.1+-FL*mmp12*Cat-7His, pCDNA3.1+-ic*mmp12*Cat-7His were transfected into 10x15cm tissue culture dishes of 90% confluent 293T cells seeded the day before, with 810mg polyethylenimine (Polyscience), respectively. 48h later, cells were lysed with 1% Triton-X100 in 0.5x phospho-buffered saline (PBS) supplemented with 1mM Phenylmethanesulfonyl Fluoride (PMSF). Cleared cell lysate were incubated with 2.5ml Ni-NTA agarose beads (Qiagen) for 1h at 4°C with 10mM imidazole in phosphate buffer containing 300mM NaCl, PH = 8, then column washed (20mM imidazole in same buffer) and eluted (250mM imidazole in same buffer) in native conditions according to manufacturer's instructions. The eluted material was switched to PBS and concentrated to ~50µL at 4^{o}C with Amicon Ultra centrifugal filters (10kD cutoff, Millipore).

Primary lung fibroblast cell culture
Primary lung fibroblast cell culture was performed as described previously (Seluanov et al., 2010). Briefly, WT and *mmp12* mutant mice of matching age were anesthetized with isoflurane and sacrificed by cervical dislocation. Lungs were removed and cut into small pieces with a stabbing knife under a dissection hood, then digested with Trypsin-EDTA in HBSS (Sigma) for 20min and further dissociated by passing 10 times through a 1000µl micropipette tip. The dissociated cells and tissue chunks were plated on 10cm tissue culture dishes (one per mouse) in DMEM supplemented with 20%FBS and 1% pen-strep. One week later, cells were passaged 1:4 and plated in EMEM supplemented with 20%FBS, 0.584mg/ml glutamine, and 1% pen-strep. Cells were then passaged at confluency up to two times before being lysed at the same degree of confluency (70%).

Immunohistochemistry on cryostat sections
Brains from mice younger than P14 were fixed in 4% PFA overnight at 4°C. Fixed tissue was washed 3 times with PBS and cryoprotected with 30% sucrose in PBS, then frozen at -80°C in Tissue-Tek OCT Compound (Sakura). Coronal sections of 20µm were cut by cryostat (Leica CM1900) at -18^{o}C and mounted on glass slides, air-dried for 1h before being stored in -80^{o}C. Antigen retrieval was performed with Dako Cytomation Target Retrieval solution, Citrate pH 6 (Dako). Sections were blocked in 10% donkey serum in PBS with 0.5% TritonX-100 for 1h, then incubated with 1° antibodies diluted in blocking solution at 4°C overnight. After washing with PBS, sections were incubated with 2° antibodies diluted in blocking solution at room temperature for two hours.

Sections were then washed with PBS with 0.1% TritonX-100 for 3 times and then stained with DAPI for 10 min. Sections were mounted in SlowFade Gold Antifade and coverslips.

References

Colognato, H., Ramachandrappa, S., Olsen, I.M., and ffrench-Constant, C. (2004). Integrins direct Src family kinases to regulate distinct phases of oligodendrocyte development. J Cell Biol *167*, 365-375.

Hand, R., Bortone, D., Mattar, P., Nguyen, L., Heng, J.I., Guerrier, S., Boutt, E., Peters, E., Barnes, A.P., Parras, C.*, et al.* (2005). Phosphorylation of Neurogenin2 specifies the migration properties and the dendritic morphology of pyramidal neurons in the neocortex. Neuron *48*, 45-62.

Kissler, S., Stern, P., Takahashi, K., Hunter, K., Peterson, L.B., and Wicker, L.S. (2006). In vivo RNA interference demonstrates a role for Nramp1 in modifying susceptibility to type 1 diabetes. Nat Genet *38*, 479-483.

Seluanov, A., Vaidya, A., and Gorbunova, V. (2010). Establishing primary adult fibroblast cultures from rodents. J Vis Exp.